

Functional identity of hypothalamic melanocortin neurons depends on Tbx3

Carmelo Quarta^{1,2,3,4,22}, Alexandre Fiset^{1,2,22}, Yanjun Xu^{1,2,5}, Gustav Collidén^{1,2}, Beata Legutko^{1,2}, Yu-Ting Tseng^{6,7}, Alexander Reim⁸, Michael Wierer⁸, Maria C. De Rosa⁹, Valentina Klaus^{1,2,5}, Rick Rausch⁹, Vidhu V. Thaker¹⁰, Elisabeth Graf¹¹, Tim M. Strom¹¹, Anne-Laure Poher^{1,2}, Tim Gruber^{1,2}, Ophélie Le Thuc^{1,2}, Alberto Cebrian-Serrano^{1,2}, Dhiraj Kabra^{1,2}, Luigi Bellochio^{12,13}, Stephen C. Woods¹⁴, Gert O. Pflugfelder¹⁵, Rubén Nogueiras^{16,17}, Lori Zeltser¹⁸, Ilona C. Grunwald Kadow¹⁹, Anne Moon^{20,21}, Cristina García-Cáceres^{1,2}, Matthias Mann¹⁶, Mathias Treier^{6,7}, Claudia A. Doege¹⁷ and Matthias H. Tschöp^{1,2,5*}

Heterogeneous populations of hypothalamic neurons orchestrate energy balance via the release of specific signatures of neuropeptides. However, how specific intracellular machinery controls peptidergic identities and function of individual hypothalamic neurons remains largely unknown. The transcription factor T-box 3 (Tbx3) is expressed in hypothalamic neurons sensing and governing energy status, whereas human TBX3 haploinsufficiency has been linked with obesity. Here we demonstrate that loss of Tbx3 function in hypothalamic neurons causes weight gain and other metabolic disturbances by disrupting both peptidergic identity and plasticity of Pomc/Cart and Agrp/Npy neurons. These alterations are observed after loss of Tbx3 in both immature hypothalamic neurons and terminally differentiated murine neurons. We further establish the importance of Tbx3 for body weight regulation in *Drosophila melanogaster* and show that TBX3 is implicated in the differentiation of human embryonic stem cells (hESC) into hypothalamic Pomc neurons. Our data indicate that Tbx3 directs the terminal specification of neurons as functional components of the melanocortin system and is required for maintaining their peptidergic identity. In summary, we report the discovery of a mechanistic key process underlying the functional heterogeneity of hypothalamic neurons governing body weight and systemic metabolism.

Energy-sensing neuronal populations of the hypothalamic arcuate nucleus (ARC), including proopiomelanocortin (Pomc)- and agouti-related protein (Agrp)-expressing neurons, release specific neuropeptides that control energy homeostasis by modulating appetite and energy expenditure. Dysregulated activity of these neurons, which constitute key components of the melanocortin system¹, is causally linked with energy imbalance and obesity^{2–4}. Considering the constantly changing input into these neurons throughout development and adult life, an intricate intracellular regulatory network must be in place to accommodate plasticity adjustments (as an adequate response to energy state) as well as maintenance of cell identity. Whether extrinsic signals can induce

in vivo reprogramming of neuropeptidergic identity has not been resolved, partly because of the limited knowledge of the intracellular factors involved.

To identify genes implicated in maintenance of ARC neuronal identity and energy-sensing function, we took advantage of cell-specific transcriptomic approaches that allow profiling of subpopulations of hypothalamic neurons under basal and metabolically stimulated conditions. We cross-referenced publicly available analysed datasets from phosphorylated ribosome profiling⁵, translating ribosome affinity purification (TRAP)-based sequencing of leptin-receptor-expressing neurons⁶, and single-cell sequencing⁷. We determined that the transcription factor termed Tbx3 is expressed

¹Institute for Diabetes and Obesity, Helmholtz Diabetes Center, Helmholtz Zentrum München, Neuherberg, Germany. ²German Center for Diabetes Research (DZD), Neuherberg, Germany. ³INSERM, Neurocentre Magendie, Physiopathologie de la Plasticité Neuronale, U1215, Bordeaux, France. ⁴University of Bordeaux, Neurocentre Magendie, Physiopathologie de la Plasticité Neuronale, Bordeaux, France. ⁵Division of Metabolic Diseases, Technische Universität München, Munich, Germany. ⁶Cardiovascular and Metabolic Sciences, Max Delbrück Center for Molecular Medicine in the Helmholtz Association (MDC), Berlin, Germany. ⁷Charité-Universitätsmedizin Berlin, Berlin, Germany. ⁸Department of Proteomics and Signal Transduction, Max-Planck Institute of Biochemistry, Martinsried, Germany. ⁹Naomi Berrie Diabetes Center, Columbia Stem Cell Initiative, Department of Pediatrics, Columbia University, New York, NY, USA. ¹⁰Naomi Berrie Diabetes Center, Division of Molecular Genetics, Department of Pediatrics, Columbia University, New York, NY, USA. ¹¹Institute of Human Genetics, Helmholtz Zentrum München, Neuherberg, Germany. ¹²INSERM U1215, NeuroCentre Magendie, Bordeaux, France. ¹³Université de Bordeaux, NeuroCentre Magendie, Bordeaux, France. ¹⁴University of Cincinnati College of Medicine, Department of Psychiatry and Behavioral Neuroscience, Metabolic Diseases Institute, Cincinnati, OH, USA. ¹⁵Institute of Developmental and Neurobiology, Johannes Gutenberg-University, Mainz, Germany. ¹⁶Department of Physiology, CIMUS, University of Santiago de Compostela-Instituto de Investigación Sanitaria, Santiago de Compostela, Spain. ¹⁷CIBER Fisiopatología de la Obesidad y Nutrición (CIBERObn), Madrid, Spain. ¹⁸Naomi Berrie Diabetes Center, Columbia Stem Cell Initiative, Department of Pathology and Cell Biology, Columbia University, New York, NY, USA. ¹⁹Technical University of Munich, School of Life Sciences, ZIEL - Institute for Food and Health, Freising, Germany. ²⁰Department of Molecular and Functional Genomics, Geisinger Clinic, Danville PA, USA. ²¹Departments of Pediatrics and Human Genetics, University of Utah School of Medicine, Salt Lake City, UT, USA. ²²These authors contributed equally: Carmelo Quarta and Alexandre Fiset. *e-mail: matthias.tschop@helmholtz-muenchen.de

with unique abundance in hypothalamic neuronal populations critically involved in energy balance regulation, including ghrelin- and leptin-responsive cells^{5,6}, and that its expression is regulated by scheduled feeding⁵.

Although *Tbx3* is known to influence proliferation⁸, fate commitment and differentiation^{9–11} of several non-neuronal cell types, its functional role during neuronal development or in post-mitotic neurons located in the CNS is currently uncharted. Intriguingly, this factor appears to be selectively expressed in the ARC in the adult murine hypothalamus¹². Moreover, *TBX3* mutations in humans have been described to cause Ulnar–Mammary syndrome (UMS), exhibiting hallmark symptoms theoretically consistent with ARC neuron dysfunction, including impaired puberty, deficiency in growth hormone production and obesity^{13,14}.

Thus, we hypothesized that *Tbx3* in ARC neurons may control neuronal identity and consequently be of critical relevance for systemic energy homeostasis. To test this hypothesis, we explored the functional role of *Tbx3* in both murine and human hypothalamic neurons and investigated whether loss of neuronal *Tbx3* impacts systemic energy homeostasis in mice and in *Drosophila melanogaster*.

We here report that *Tbx3* directs postnatal fate and is critical for defining peptidergic identity of both immature and terminally differentiated murine melanocortin neurons, a biological process that is essential for regulation of energy balance.

Results

***Tbx3* expression profile in CNS and pituitary.** To characterize *Tbx3* expression in the central nervous system (CNS), we generated a targeted knock-in mouse model in which the Venus reporter protein is expressed under the control of the *Tbx3* locus (*Tbx3*-Venus mice) (Supplementary Fig. 1). Two areas of the brain displayed a detectable Venus signal, the ARC (Fig. 1a) and the nucleus of the solitary tract (Supplementary Fig. 1), both of which are important in the regulation of systemic metabolism^{15,16}. This hypothalamic expression pattern was confirmed via qRT-PCR (Supplementary Fig. 1) and anti-*Tbx3* immunohistochemistry (Supplementary Fig. 1), using an antibody validated in house with *Tbx3*-deficient embryos (Supplementary Fig. 1). All Venus-positive cells in the ARC and NTS of *Tbx3*-Venus mice coexpressed *Tbx3*, as assessed by immunohistochemistry (Supplementary Fig. 1), and the model was further validated via Southern blot analysis (Supplementary Fig. 1). This underlines the quality of the newly developed transgenic model.

To further address the cell-specific expression profile of *Tbx3*, we performed bioinformatic-based reanalysis of a publicly available single-cell RNA sequencing (RNA-seq) dataset from the ARC⁷. Our analysis demonstrated overlap of *Tbx3* with neurons expressing *Pomc*, *Agrp*, kisspeptin (*Kiss*), and somatostatin (Fig. 1b and Supplementary Fig. 1), in addition to overlapping with the transcriptional profile of tanycytes, the ‘gateway’ cells to the metabolic hypothalamus¹⁷ (Supplementary Fig. 1).

Neuroanatomical analysis in *Tbx3*-Venus mice demonstrated *Tbx3* (Venus) expression in almost all ARC *Pomc* neurons (Fig. 1c) and NTS *Pomc* neurons (Supplementary Fig. 1), with a comparable pattern of expression from embryonic (E18.5) to postnatal life (P0, P4 and adults) (Fig. 1d), indicating that *Tbx3* expression in *Pomc* neurons is switched on embryonically and maintained throughout adult life. As suggested by the analysis of the single-cell RNA-seq data from the cells from Arc-Median eminence, a considerable fraction of *Tbx3*-positive cells do not express *Pomc*. *Tbx3* transcripts have been previously observed within the pituitary gland¹⁸. We found that *Tbx3* (Venus) expression was restricted to the posterior pituitary, and that no signal was observed in *Pomc*-expressing cells of the anterior pituitary (Supplementary Fig. 1). Moreover, no signs of *Tbx3* (Venus) expression were detected in glial fibrillary acidic protein (GFAP)-positive astrocytes (Supplementary Fig. 1) or in

microglia (Iba1-positive glial cells) (Supplementary Fig. 1), whereas a substantial number of *Tbx3* (Venus)-positive cells coexpressed the tanycyte and reactive astrocyte marker vimentin (Supplementary Fig. 1), in agreement with results from single-cell sequencing analysis (Supplementary Fig. 1).

Thus, within the CNS, *Tbx3* is expressed in both neuronal and non-neuronal cells known to impact energy homeostasis.

Loss of *Tbx3* in hypothalamic neurons promotes obesity. ARC neurons detect changes in energy status, via both direct and indirect sensing of circulating nutrients and hormones, and accordingly modulate their activity to maintain energy balance¹⁶. Overnight fasting significantly decreased hypothalamic *Tbx3* mRNA levels in the ARC of C57BL/6J mice, whereas refeeding partially restored *Tbx3* expression (Fig. 1e). This finding suggests that changes in hypothalamic *Tbx3* levels are likely to be involved in the control of systemic metabolism. To test this notion, we used a viral-based approach to selectively ablate *Tbx3* via Cre-LoxP recombination (adeno-associated virus (AAV)-Cre) from the mediobasal hypothalamus (MBH) of 12-week-old *Tbx3*^{loxP/loxP} littermate mice (Supplementary Fig. 2).

AAV-Cre-treated mice developed pronounced obesity over the course of 7 weeks, with elevated cumulative food intake and higher fat mass relative to control mice (AAV-green fluorescent protein (GFP)-treated *Tbx3*^{loxP/loxP} mice), whereas no difference was observed in lean mass (Fig. 1f–i). Indirect calorimetry did not reveal changes in hourly uncorrected energy expenditure (Fig. 1j), nor in the relationship between total uncorrected energy expenditure and body weight, as demonstrated by analysis of covariance (ANCOVA)¹⁹ (Fig. 1k). Although the average respiratory exchange ratio (RER) was not altered in AAV-Cre-treated mice, these mice displayed metabolic inflexibility relative to controls, as indicated by a flat RER with minimal diurnal fluctuations (Fig. 1l,m).

We next asked whether loss of function of *Tbx3* selectively in either *Agrp* or *Pomc* neurons would recapitulate the obesity-prone phenotype observed in the MBH loss-of-function model. No difference in body weight, food intake, glucose tolerance, fat or lean mass was observed in littermate mice bearing a conditional deletion of *Tbx3* in *Agrp*-expressing neurons (*Agrp*-Cre;*Tbx3*^{loxP/loxP}) relative to controls (Fig. 2a–e). The quality of this previously validated²⁰ transgenic model was confirmed by the presence of reduced *Tbx3* mRNA levels in ARC homogenates (Supplementary Fig. 2), together with a specific reduction of *Tbx3* expression within *Npy*-positive neurons (Supplementary Fig. 2).

In contrast, mice bearing *Tbx3* deletion in *Pomc*-expressing cells²¹ (*Pomc*-Cre;*Tbx3*^{loxP/loxP}) displayed elevated body weight relative to control littermates, independently from changes in food intake (Fig. 2f,g). They also had glucose intolerance (Fig. 2h) and increased fat and lean mass (Fig. 2l,j). Indirect calorimetry demonstrated similar hourly energy expenditure, in spite of higher body weight (Fig. 2k), and further revealed a reduction in energy expenditure with respect to body weight in *Pomc*-Cre;*Tbx3*^{loxP/loxP} mice relative to controls (Fig. 2l), suggesting that lower systemic energy dissipation may contribute to their obese phenotype. These mice also displayed higher average RER (Fig. 2m,n), indicating that lower lipid utilization might favour the increased adiposity of these mice. A significant reduction in *Tbx3* mRNA levels was observed in the hypothalamus of *Pomc*-Cre;*Tbx3*^{loxP/loxP} mice, whereas no changes in *Tbx3* mRNA levels were detected in extra-hypothalamic sites expressing *Pomc*, including the pituitary and adrenals (Supplementary Fig. 2). This transgenic model was further validated via costaining between *Tbx3* and a Cre-dependent membrane GFP reporter, an analysis that revealed blunted *Tbx3* immunoreactivity in Cre-positive neurons of *Pomc*-Cre;*Tbx3*^{loxP/loxP} mice relative to controls (Supplementary Fig. 2). Thus, the metabolic alterations observed in this model are attributable to the specific deletion of *Tbx3* in *Pomc* neurons located in the CNS. Collectively, these data

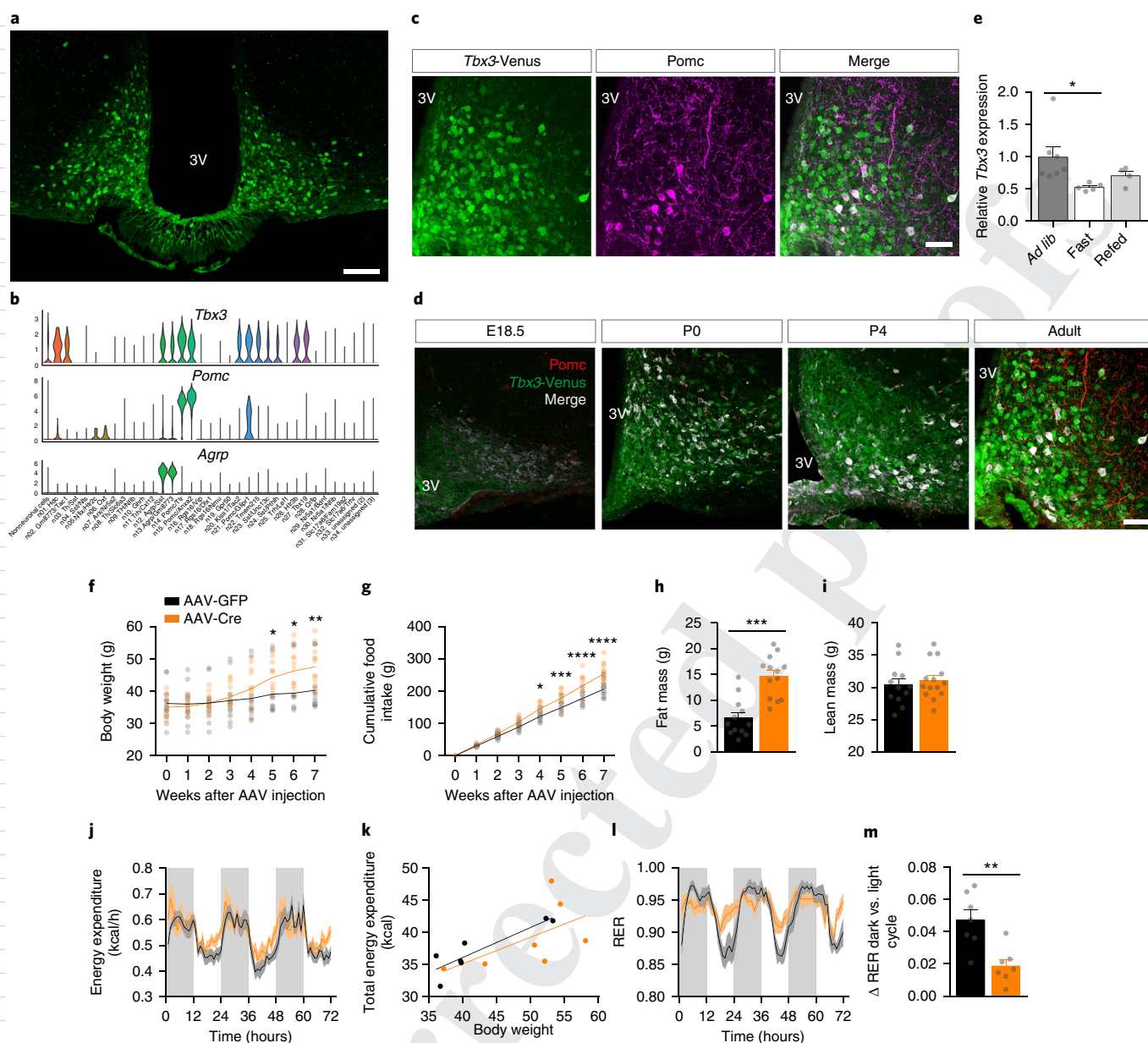


Fig. 1 | Loss of *Tbx3* in hypothalamic neurons promotes obesity. **a**, Representative image depicting *Tbx3*-positive neurons in the ARC of *Tbx3*-Venus mice, enhanced with GFP immunohistochemistry. 3V, third ventricle. Scale bar, 100 μ m. **b**, Violin plots depicting expression of *Tbx3*, *Pomc* and *AgRP* across neuronal clusters identified by Campbell et al⁷. Of the 21,086 cells analysed, 13,079 were identified as neurons, and 8,007 were identified as non-neurons on the basis of expression of the canonical neuronal marker *Tubb3*. The width of the violin plot at different levels of the log-transformed and scaled expression levels indicates high levels of expression of *Tbx3* in neuronal clusters 14 (*Pomc*/*Ttr*, $n=512$), 15 (*Pomc*/*Anxa2*, $n=369$) and 21 (*Pomc*/*Glipr1*, $n=310$) compared with that of the other neuronal clusters. **c**, Colocalization between *Tbx3*-Venus and *Pomc* in the ARC of *Tbx3*-Venus mice, assessed by immunohistochemistry. Scale bar, 50 μ m. **d**, Colocalization between *Tbx3*- and *Pomc*-expressing cells by immunohistochemistry in *Tbx3*-Venus mice during embryonic (E18.5), neonatal (P0, P4), and adult life (shown in **c**). **e**, Quantification of *Tbx3* mRNA levels by qRT-PCR in ARC micropunches isolated from adult (12-week-old) C57BL/6J mice after 24 h of fasting ($n=5$) or 24 h of fasting followed by 6 h of refeeding ($n=4$), relative to mice fed ad libitum ($n=7$). **f, g**, Body weight change (**f**) and cumulative food intake (**g**) in adult *Tbx3*^{loxP/loxP} mice after stereotaxic injection in the MBH of AAV-Cre ($n=14$) or AAV-GFP ($n=12$) particles. **h, i**, Fat mass of AAV-Cre-treated ($n=13$) or AAV-GFP-treated ($n=12$) *Tbx3*^{loxP/loxP} mice, 7 weeks after surgery. **i**, Lean mass of AAV-Cre-treated ($n=14$) or AAV-GFP-treated ($n=12$) *Tbx3*^{loxP/loxP} mice, 7 weeks after surgery. **j, k**, Hourly energy expenditure (**j**) and total uncorrected energy expenditure correlated to body weight (**k**) in AAV-Cre-treated ($n=7$) or AAV-GFP-treated ($n=7$) *Tbx3*^{loxP/loxP} mice 4 weeks after surgery. **l, m**, Hourly RER (**l**) and Δ RER averaged between night and day cycles (**m**) in AAV-Cre-treated ($n=7$) or AAV-GFP-treated ($n=7$) *Tbx3*^{loxP/loxP} mice 4 weeks after surgery. In **k**, individual data are presented, and lines depict the fitted regression. In all other analyses, data are mean \pm s.e.m. In **e**, * $P=0.0476$ relative to ad libitum feeding using ANOVA followed by Tukey's post-test. In **f**, * $P=0.0177$, ** $P=0.0095$ using ANOVA followed by Sidak's post-test. In **g**, ** $P=0.0028$, *** $P=0.0001$ and **** $P<0.0001$ using ANOVA followed by Sidak's post-test. In **h** and **m**, *** $P<0.0001$ and ** $P=0.0029$ and using a two-tailed t test. The experiments in **a** and **c** were repeated more than three independent times with similar results. The experiments in **d** were performed once, with several samples showing similar results.

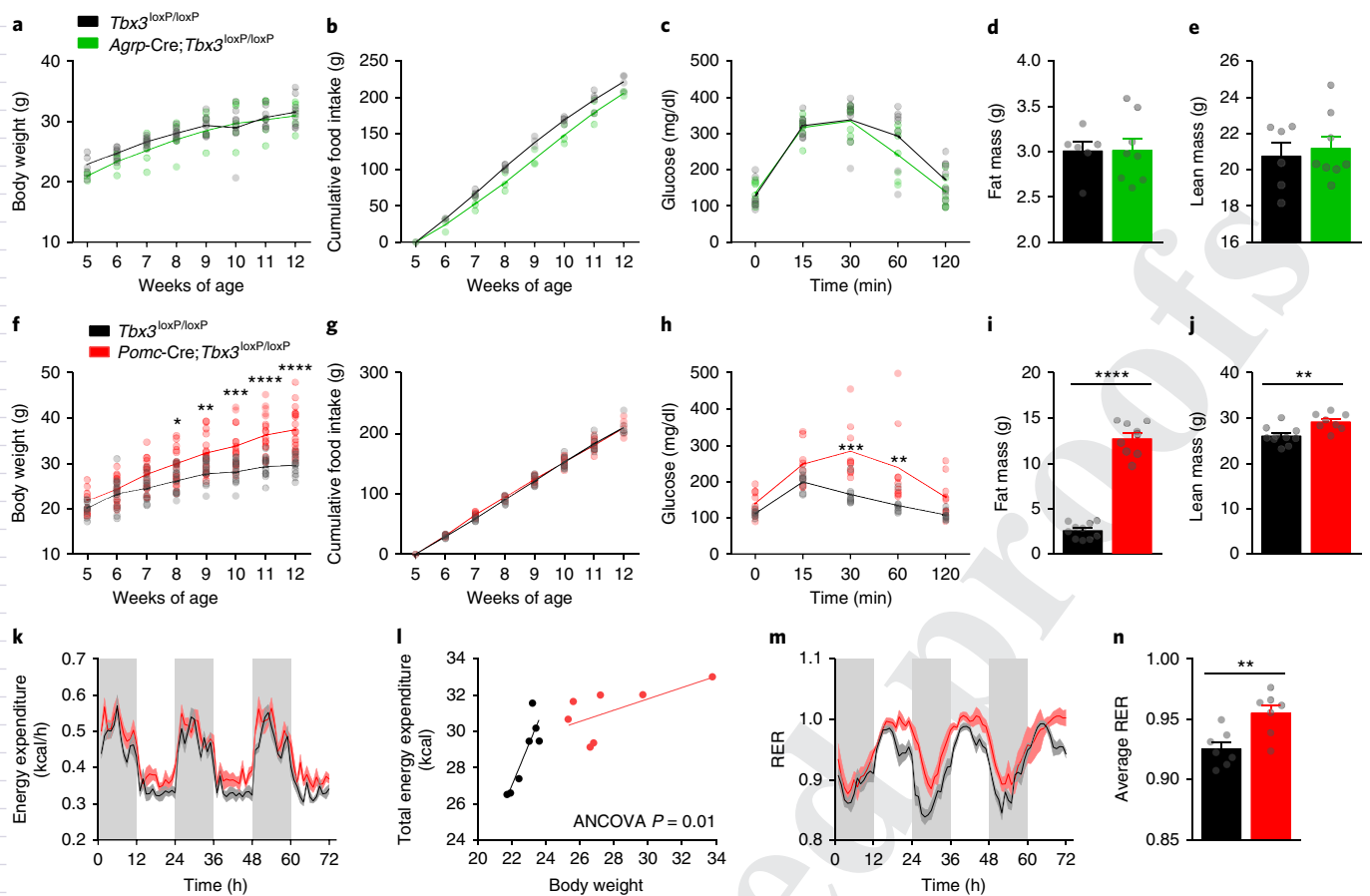


Fig. 2 | Loss of *Tbx3* in *Pomc* but not *Agrp* neurons triggers obesity. **a**, Body weight in *Agrp-Cre;Tbx3^{loxP/loxP}* mice ($n=5$) relative to control littermates ($n=8$). **b**, Cumulative food intake in *Agrp-Cre;Tbx3^{loxP/loxP}* mice ($n=3$) relative to control littermates ($n=4$). **c**, Glucose tolerance test in adult *Agrp-Cre;Tbx3^{loxP/loxP}* mice ($n=7$) relative to control littermates ($n=8$). **d, e**, Fat mass (**d**) and lean mass (**e**) in adult *Agrp-Cre;Tbx3^{loxP/loxP}* mice ($n=8$) relative to control littermates ($n=6$). **f**, Body weight in *Pomc-Cre;Tbx3^{loxP/loxP}* mice ($n=18$) relative to control littermates ($n=11$). **g**, Cumulative food intake in *Pomc-Cre;Tbx3^{loxP/loxP}* mice ($n=7$) relative to control littermates ($n=7$). **h**, Glucose tolerance test in adult *Pomc-Cre;Tbx3^{loxP/loxP}* mice ($n=9$) relative to control littermates ($n=8$). **i, j**, Fat mass (**i**) and lean mass (**j**) in adult *Pomc-Cre;Tbx3^{loxP/loxP}* mice ($n=9$) relative to control littermates ($n=10$). **k–n**, Hourly energy expenditure (**k**) and energy expenditure correlated to body weight (**l**), hourly RER (**m**), and average RER values (**n**), in 7-week-old *Pomc-Cre;Tbx3^{loxP/loxP}* mice ($n=7$) relative to control littermates ($n=7$). Data in **a–k, m, n**, are mean \pm s.e.m. In **f**, * $P=0.02$, ** $P=0.003$, *** $P=0.0001$, **** $P<0.0001$ using ANOVA followed by Sidak's post-test. In **h**, ** $P=0.001$, *** $P=0.0002$ using ANOVA followed by Sidak's post-test. In **i, j**, **** $P<0.0001$ and ** $P=0.0035$ using two-tailed t test. In **n**, ** $P=0.0055$ using two-tailed t test.

demonstrate that ablation of *Tbx3* in ARC neurons has profound functional consequences on energy balance and that most of these metabolic alterations can be reproduced after specific deletion of this gene in *Pomc*-positive neurons located in the brain.

Loss of *Tbx3* impairs the postnatal melanocortin system.

Although *Tbx3* is known to control cell cycle and programming of highly proliferative stem cells and cancer cells^{9–11,22}, its functional role in neurons has remained unexplored. To investigate possible biological mechanisms underlying the metabolic phenotypes observed, we performed *Tbx3*-focused RNA sequencing and proteomic analyses in hypothalamic tissue, as well as in primary hypothalamic cultures. The impact of *Tbx3* deletion on transcription in hypothalamic neurons was assessed using primary neurons isolated from *Tbx3^{loxP/loxP}* mice and infected with adenoviral (Ad) particles carrying the coding sequence for Cre recombinase (Ad-Cre) or GFP (Ad-GFP) as a control (Supplementary Fig. 3), an approach that effectively allows knockdown of *Tbx3* (Supplementary Fig. 3) in the absence of cell toxicity (Supplementary Fig. 3). Because we had found the most important in vivo metabolic effects with *Tbx3* deletion uniquely within *Pomc*-expressing cells, we performed RNA

sequencing of the wild-type (WT) and *Tbx3*-knockout (*Tbx3*-KO) primary hypothalamic cultures and identified genes that were both differentially expressed in this in vitro model and known to be expressed in *Pomc* neurons. This analysis highlighted 449 transcripts that were differentially expressed (243 downregulated, 206 upregulated). Unbiased pathway analysis revealed that *Tbx3* deletion significantly downregulated the expression of genes controlling cellular proliferation, differentiation and determination of cellular fate (Supplementary Fig. 3). In turn, several genes linked with intracellular metabolic pathways were upregulated, albeit in a less significant way (Supplementary Fig. 3). To complement this unbiased approach, in silico analysis of the genomic loci coding for *Pomc*, *Cart* and *Agrp* for potential *Tbx3*-binding sites (T-box binding motifs) was performed²³. Potential *Tbx3*-binding sites were found in all three genes, suggesting that *Tbx3* could alter their transcription directly (Supplementary Fig. 3). To further explore the molecular machinery linked with *Tbx3* in hypothalamic neurons, we performed immunoprecipitation of *Tbx3* from adult C57BL/6J mouse hypothalami, then used mass spectrometry to identify *Tbx3*-interacting proteins. 142 proteins were significantly enriched by *Tbx3* precipitation (Supplementary Fig. 3 and Supplementary

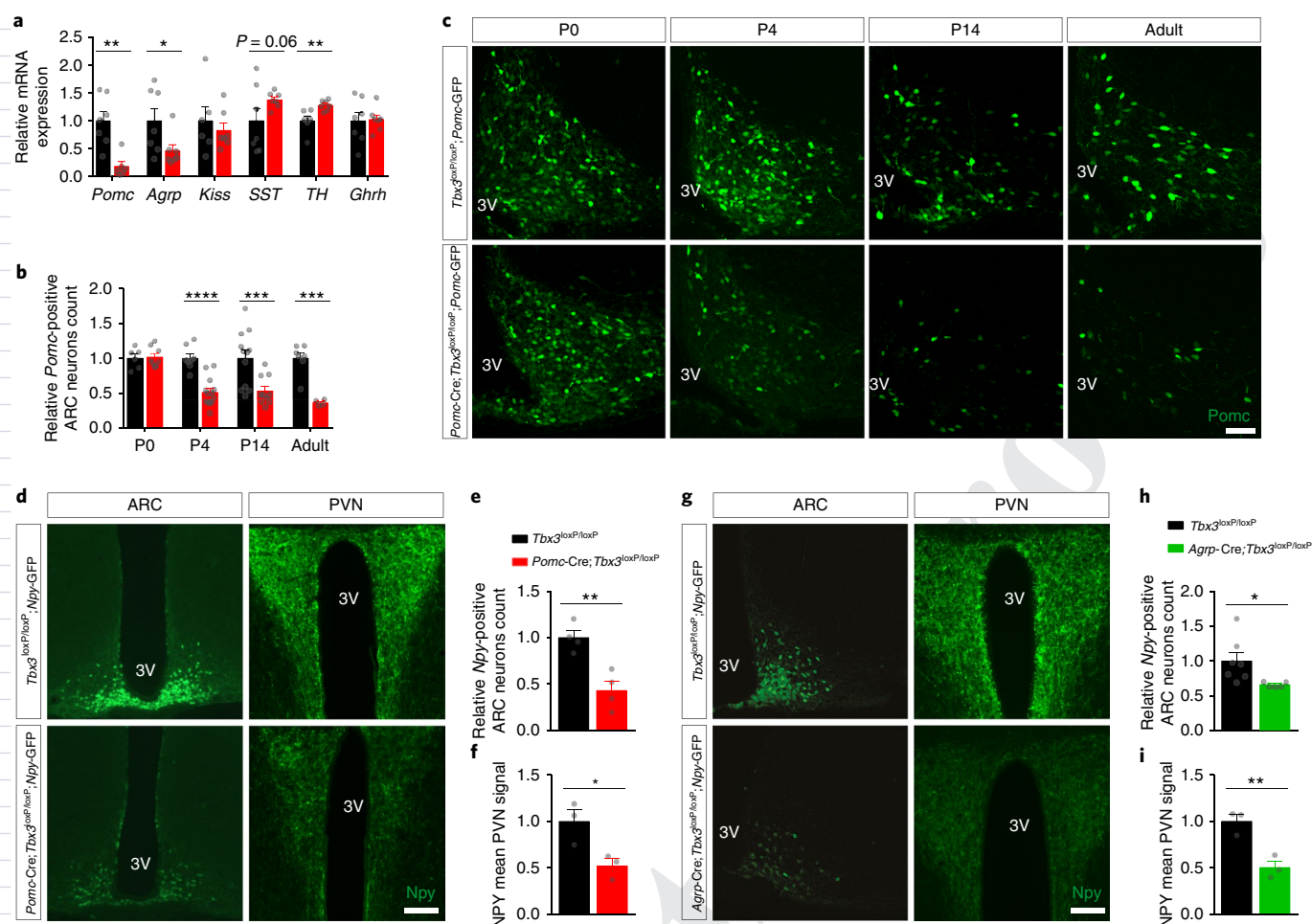


Fig. 3 | Loss of *Tbx3* impairs the postnatal melanocortin system. **a**, Quantification of enzyme and neuropeptide mRNA levels by qRT-PCR in ARC micropunches isolated from adult (12 week old) *Pomc-Cre;Tbx3^{loxP/loxP}* mice ($n = 7$) and control *Tbx3^{loxP/loxP}* littermates ($n = 7$). *Kiss*, kisspeptin; *SST*, somatostatin; *TH*, tyrosine hydroxylase; *Ghrr*, growth-hormone-releasing hormone. **b,c**, Quantification (**b**) and representative images (**c**) of the relative number of *Pomc*-expressing neurons in the ARC of *Pomc-Cre;Tbx3^{loxP/loxP};Pomc-GFP* mice and in control littermates (*Tbx3^{loxP/loxP};Pomc-GFP*) at different stages of neonatal life and in adult animals. *Tbx3^{loxP/loxP};Pomc-GFP*: $n = 6$ (P0); $n = 8$ (P4); $n = 12$ (P14); $n = 7$ (adult). *Pomc-Cre;Tbx3^{loxP/loxP};Pomc-GFP*: $n = 8$ (P0); $n = 13$ (P4); $n = 10$ (P14); $n = 4$ (adult). **d,e**, Representative images (**d**) and relative quantification (**e**) of *Npy*-positive neurons in the ARC of adult *Pomc-Cre;Tbx3^{loxP/loxP};Npy-GFP* mice ($n = 4$) and control littermates (*Tbx3^{loxP/loxP};Npy-GFP*, $n = 4$). **f**, *Npy*-positive neuronal fibres in the PVN of adult *Pomc-Cre;Tbx3^{loxP/loxP};Npy-GFP* mice ($n = 3$) and control littermates (*Tbx3^{loxP/loxP};Npy-GFP*, $n = 3$). **g,h**, Representative images (**g**) and relative quantification (**h**) of *Npy*-positive neurons in the ARC of adult *Agrp-Cre;Tbx3^{loxP/loxP};Npy-GFP* mice ($n = 5$) and control littermates (*Tbx3^{loxP/loxP};Npy-GFP*, $n = 7$). **i**, *Npy*-positive neuronal fibres in the PVN of adult *Agrp-Cre;Tbx3^{loxP/loxP};Npy-GFP* mice ($n = 3$) and control littermates (*Tbx3^{loxP/loxP};Npy-GFP*, $n = 3$). 3V, third ventricle. Scale bar in **c**, 50 μm ; scale bars in **d-g**, 100 μm . Data **a,b,e,f** and **h,i**, are mean \pm s.e.m. In **a**, ** $P = 0.0017$ (*Pomc*), ** $P = 0.0097$ (*TH*), * $P = 0.0049$ using two-tailed t test. In **b**, **** $P < 0.0001$ (P4), *** $P = 0.0032$ (P14), *** $P = 0.0002$ (adult) using two-tailed t test. In **e,f**, ** $P = 0.0043$, * $P = 0.034$ using two-tailed t test. In **h,i**, * $P = 0.04$, ** $P = 0.0087$ using two-tailed t test. The experiments in **c** were repeated more than three independent times with similar results. The experiments in **d** and **g** were repeated two independent times with similar results.

Table 2), including previously known *Tbx3* interactors such as *Kif21* (ref. 24), *AES*²⁵ and *Tollip*²⁶. Pathway analysis of these interacting proteins highlighted their role in several processes, notably including inter- and intracellular signalling and neuronal development (Supplementary Fig. 3). These genomic and proteomic data led us to test the hypothesis that a lack of *Tbx3* in the ARC might interfere with the cellular fate and differentiation stage of these neurons and, therefore, impact their peptidergic profile, in addition to potentially affecting neuropeptide generation via direct transcriptional actions.

Accordingly, we measured *Pomc* and *Agrp* mRNA expression in WT and *Tbx3*-KO primary hypothalamic neurons by means of qRT-PCR. Both transcripts were significantly downregulated after Ad-Cre-mediated *Tbx3* deletion (Supplementary Fig. 4). These changes were reproducible in vivo, as we found significantly lower expression levels of *Pomc* and *Agrp* mRNA in the ARC of

Pomc-Cre;Tbx3^{loxP/loxP} mice relative to those in control littermates (Fig. 3a). No changes in *Kiss* or growth hormone releasing hormone (*Ghrr*) mRNA levels were observed in these animals, whereas mRNA levels of tyrosine hydroxylase were elevated, and there was a trend toward elevated levels of somatostatin (Fig. 3a). To explore whether these changes in their peptidergic expression profile were caused by neurodevelopmental alterations, *Pomc-Cre;Tbx3^{loxP/loxP}* mice were crossed with *Pomc-GFP* reporter animals in order to precisely quantify *Pomc*-expressing cells during both embryonic and postnatal life, when ARC-*Pomc* neurons are generated and acquire their terminal peptidergic identity^{27,28}. No difference in *Pomc* neuronal cell number was detected in this model at embryonic day (E) 14.5, E15.5, or E18.5, implying normal neuronal generation in utero (Supplementary Fig. 4). No change in *Pomc* counts was observed at postnatal day (P) 0, whereas a substantial reduc-

tion in the number of *Pomc*-positive neurons was found at P4, and this relative decrement remained at P14 and 12 weeks (adult) (Fig. 3b,c). Despite progressive loss of *Pomc* expression at P2 and P4, no significant apoptotic activity was observed in this region (Supplementary Fig. 4), nor did we detect any proliferation leading to new *Pomc*-positive neurons between P0 and P3, as assessed using BrdU (Supplementary Fig. 4), confirming that most *Pomc* neurons are generated during embryonic life²⁸ and suggesting that neurogenesis and/or cellular turnover do not contribute to *Tbx3*-mediated control of *Pomc* expression observed during neonatal life. Furthermore, no compensatory change was observed in the *Pomc*-processing enzymes of *Pomc-Cre;Tbx3^{loxP/loxP}* mice (Supplementary Fig. 4). Collectively, these data demonstrate that constitutive loss of *Tbx3* in *Pomc*-expressing neurons undermines the melanocortin system, likely by interfering with the proper terminal differentiation of this neuronal population during postnatal life and possibly via direct transcriptional actions.

Loss of *Tbx3* alters the peptidergic profile of *Agrp* neurons. In agreement with results from the mRNA analysis documenting reduced ARC *Agrp* mRNA (Fig. 3a), *Pomc-Cre;Tbx3^{loxP/loxP}* mice displayed a reduced number of neuropeptide Y (*Npy*)-expressing neurons (co-expressed in the vast majority of *Agrp* neurons²⁹) in the ARC (Fig. 3d,e). This was also reflected by reduced *Npy* projection density in the paraventricular nucleus of the hypothalamus (PVN) (Fig. 3d–f), as demonstrated by crossing *Pomc-Cre;Tbx3^{loxP/loxP}* mice with *Npy*-GFP reporter mice. Because a significant fraction of *Agrp* and *Npy* neurons are derived from *Pomc*-expressing cells²⁷, Cre-mediated ablation of *Tbx3* in these cells may interfere with *Agrp* and *Npy* expression in this animal model, suggesting that *Tbx3* action in *Agrp*-expressing neurons may be similarly implicated in controlling the peptidergic profile of this specific neuronal subpopulation. To test this hypothesis, we crossed *Agrp-Cre;Tbx3^{loxP/loxP}* mice with *Npy*-GFP reporter mice, and quantified the number of *Npy*-positive neurons and their neuronal projections. A significant decrease in *Npy*-positive neurons in the ARC (Fig. 3g,h) and *Npy* immunoreactivity in the PVN (Fig. 3g–i) were observed in *Agrp-Cre;Tbx3^{loxP/loxP}* mice relative to littermate controls, as well as a significant reduction in ARC *Agrp* mRNA levels (Supplementary Fig. 4). Thus, *Tbx3* action in hypothalamic ARC neurons controls the peptidergic expression profiles of different neuronal subpopulations.

***Tbx3* is critical for the differentiation of *Pomc* neurons.** To further delineate the process underlying *Tbx3*-mediated control of neuropeptide expression, we used a cell lineage approach and crossed *Pomc-Cre;Tbx3^{loxP/loxP}* mice with *ROSA^{mT/mG}* reporter mice to genetically and permanently label cells undergoing Cre-mediated recombination (via the *Pomc-Cre* driver), as well as their neuronal projections. We then quantified *Pomc* expression and assessed its colocalization with GFP, indicative of Cre-mediated recombination. The P4 *Pomc-Cre;Tbx3^{loxP/loxP};ROSA^{mT/mG}* pups had a significantly reduced number of *Pomc*-positive cells relative to controls (Fig. 4a,b; raw counts available in Supplementary Table 3), thus reproducing our previously obtained results (Fig. 3b,c). However, no change was observed in the number of neurons or in neuronal-fibre density by analysing Cre-recombined (GFP-expressing) cells (Fig. 4a–c). These data are in agreement with the absence of apoptotic events at P2–4 (Supplementary Fig. 4) and demonstrate that loss of *Tbx3* function in *Pomc*-expressing cells does not affect cellular survival or neuronal architecture during embryonic or early postnatal development. Instead, most Cre-recombined neurons in *Pomc-Cre;Tbx3^{loxP/loxP};ROSA^{mT/mG}* mice lacked *Pomc* immunoreactivity (Fig. 4a,b, arrows), suggesting that *Tbx3* ablation in *Pomc*-positive cellular populations disrupts their normal peptide-ergic identity. Such alteration in *Pomc* neuronal identity in *Pomc-Cre;Tbx3^{loxP/loxP};ROSA^{mT/mG}* was also observed in adult animals

(Fig. 4d,e, arrows; raw counts available in Supplementary Table 3). Similarly, Cre-recombined cells in *Pomc-Cre;Tbx3^{loxP/loxP};ROSA^{mT/mG}* had reduced expression of *Cart* compared with controls, indicating that the peptidergic alterations in this model are not limited to *Pomc* (Supplementary Fig. 5; raw counts available in Supplementary Table 3). A slight decrease in the number of Cre-recombined cells and in neuronal fibre density in the ARC and PVN was observed in adult *Pomc-Cre;Tbx3^{loxP/loxP};ROSA^{mT/mG}* mice compared to controls (Fig. 4d–i). We hypothesize that this finding is indicative of cellular loss in *Pomc-Cre;Tbx3^{loxP/loxP};ROSA^{mT/mG}* mice during adulthood, because this phenomenon occurs only after the peptidergic identity impairment observed at P4. We speculate that *Tbx3* deletion in hypothalamic *Pomc* neurons may impair neuronal maturation during postnatal life and that this might in turn provoke cell death in a subpopulation of neurons during the transition into adult life. On the other hand, these results could also be linked with reduced postnatal neurogenesis and/or impaired neuronal turnover of *Pomc*-positive cells in *Pomc-Cre;Tbx3^{loxP/loxP};ROSA^{mT/mG}* mice, perhaps linked with the condition of obesity observed in these animals. The concept of postnatal hypothalamic neurogenesis, however, remains controversial³⁰. These data collectively demonstrate that *Tbx3* plays a fundamental role in maintaining the identity of ARC *Pomc*-expressing cells, a process that underlies changes in the neuropeptidergic profile of these neurons and consequently in systemic energy homeostasis.

***Tbx3* controls identity and plasticity of mature *Pomc* neurons.**

Because ARC *Tbx3* levels are modulated by nutritional status in mice (Fig. 1e), we asked whether *Tbx3* in hypothalamic *Pomc* neurons might be implicated in the previously observed plastic ability of these cells to adjust *Pomc* expression and release in response to changes in nutritional status³¹. *Pomc*-positive cells and *Pomc* immunoreactivity were measured in adult *Pomc-Cre;Tbx3^{loxP/loxP};Pomc-GFP* and control animals in the ad libitum-fed condition and after exposure to a fasting–refeeding paradigm. In controls, fasting reduced *Pomc*-positive cell counts (Fig. 4j,k) and *Pomc* immunoreactivity (Supplementary Fig. 5) relative to what occurred in ad libitum-fed mice, whereas refeeding normalized *Pomc* expression, as previously reported³¹. In contrast, changes in nutritional status failed to alter *Pomc* expression in adult *Pomc-Cre;Tbx3^{loxP/loxP};Pomc-GFP* mice (Fig. 4j,k and Supplementary Fig. 5), suggesting that *Tbx3* is implicated in fine-tuning *Pomc* expression in response to energy needs. These data also suggest that *Tbx3* likely controls the peptidergic profile of fully differentiated hypothalamic neurons of adult mice. To assess this possibility, we quantified *Pomc*-positive neurons in our adult-onset model of viral-mediated hypothalamic *Tbx3* deletion. A prominent reduction of ARC *Pomc*-positive cells was observed (Fig. 4l,m), with no changes in apoptotic events (Supplementary Fig. 5), implying that loss of *Tbx3* in fully mature and specified neurons alters their peptidergic identity. To uncover whether such alteration might underlie hyperphagia, and therefore the obese phenotype observed in AAV-Cre-treated mice, we challenged these animals with intracerebroventricular (ICV) injections of the biologically active *Pomc*-derived peptide alpha-melanocyte-stimulating hormone (α -MSH) at a subeffective dose. ICV injection of this dose of α -MSH had a slight, non-significant hypophagic effect in control (AAV-GFP) mice. In contrast, this approach significantly normalised food intake in AAV-Cre-treated animals to the level of control AAV-GFP mice (Fig. 4n). Together, these results document that *Tbx3* knockdown in fully differentiated ARC neurons impairs their peptidergic expression profile under non-stimulated conditions and undermines the ability of *Pomc* neurons to adjust *Pomc* expression and release in response to changes in nutritional status. These alterations, in turn, provoke dysregulated central melanocortin tone, a blunted neuronal response to the organism's nutritional status, and ultimately, obesity.

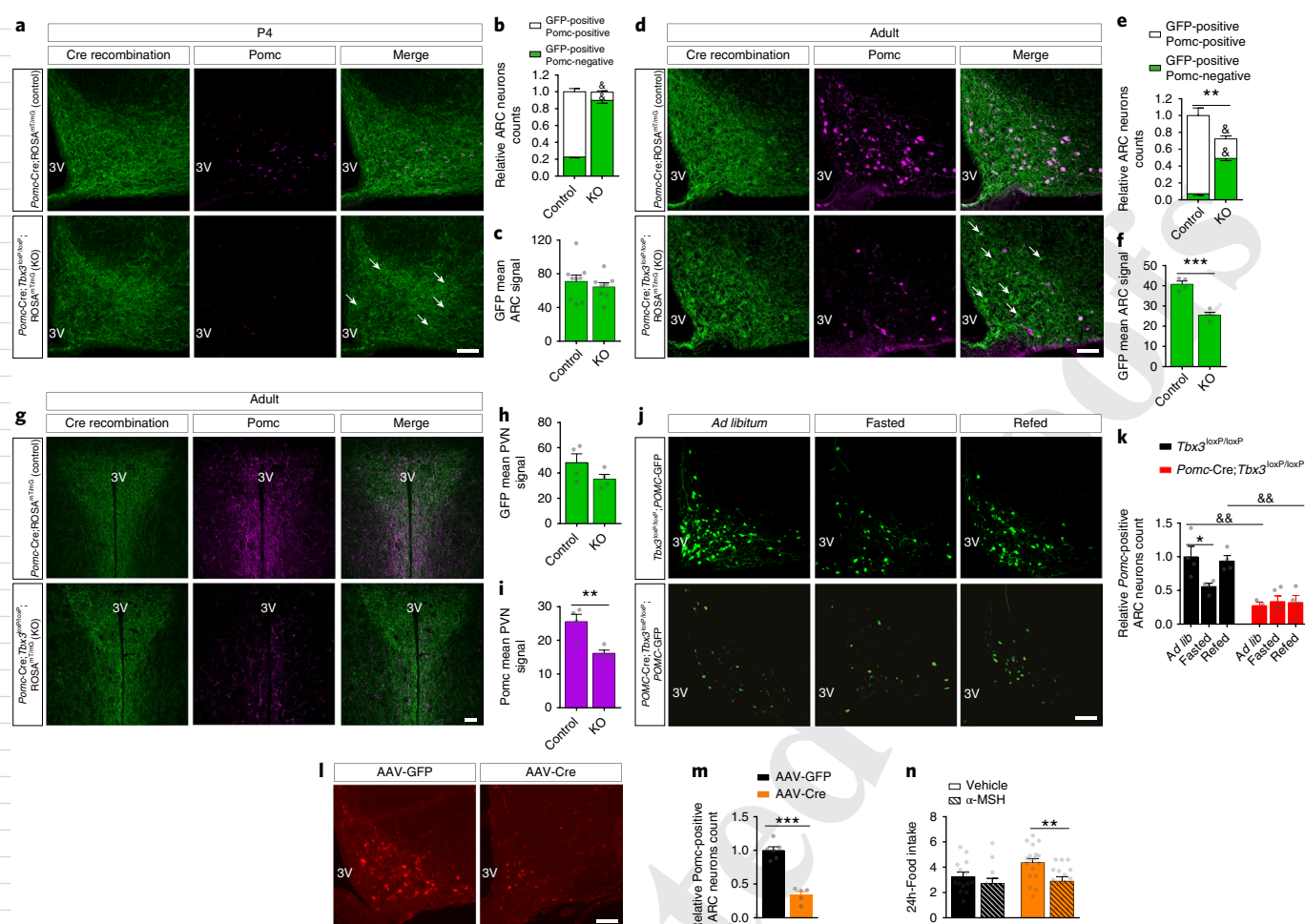


Fig. 4 | Tbx3 is critical for the differentiation of Pomc neurons. **a, b**, Representative images (**a**) and relative quantification (**b**) of GFP-expressing neurons (Cre recombination) and Pomc-positive neurons in the ARC of P4 *Pomc-Cre;Tbx3^{loxP/loxP};ROSA^{mT/mG}* mice ($n=8$) relative to controls (*Tbx3^{loxP/loxP};ROSA^{mT/mG}*, $n=9$), assessed by immunohistochemistry. Arrows depict GFP-positive/Pomc-negative cells. **c**, Relative densitometric analysis of Cre recombination (GFP immunoreactivity) in the ARC of P4 *Pomc-Cre;Tbx3^{loxP/loxP};ROSA^{mT/mG}* mice ($n=8$) and controls ($n=9$). **d, e**, Representative images (**d**) and relative quantification (**e**) of GFP-expressing neurons (Cre recombination) and Pomc-positive neurons in the ARC of adult (12-week old) *Pomc-Cre;Tbx3^{loxP/loxP};ROSA^{mT/mG}* mice ($n=4$) and controls ($n=4$), assessed by immunohistochemistry. Arrows depict GFP-positive/Pomc-negative cells. **f**, Relative densitometric analysis of Cre recombination (GFP immunoreactivity) in the ARC of adult *Pomc-Cre;Tbx3^{loxP/loxP};ROSA^{mT/mG}* mice ($n=4$) and controls ($n=4$). **g**, Representative images depicting Cre recombination (GFP immunoreactivity) and Pomc-positive neuronal fibres in the PVN of adult *Pomc-Cre;Tbx3^{loxP/loxP};ROSA^{mT/mG}* mice and controls, assessed by immunohistochemistry. **h, i**, Relative densitometric analysis of Cre recombination (GFP immunoreactivity) (**h**) and Pomc immunoreactivity (**i**) in the PVN of adult *Pomc-Cre;Tbx3^{loxP/loxP};ROSA^{mT/mG}* mice ($n=4$) and controls ($n=4$). **j, k**, Representative image (**j**) and cell number quantification (**k**) of Pomc-positive neurons in the ARC of adult *Pomc-Cre;Tbx3^{loxP/loxP};Pomc-GFP* mice or control littermates (*Tbx3^{loxP/loxP};Pomc-GFP*; $n=3$ (ad libitum); $n=5$ (fasted), $n=4$ (refed)). *Tbx3^{loxP/loxP};Pomc-GFP*; $n=4$ for each condition. **l, m**, Representative images (**l**) and relative quantification (**m**) of Pomc-expressing neurons in the ARC of adult *Tbx3^{loxP/loxP}* mice 7 weeks after AAV-Cre ($n=5$) or AAV-GFP ($n=6$) MBH injection. **n**, 24-h food intake measured in adult *Tbx3^{loxP/loxP}* mice 7 weeks after AAV-Cre or AAV-GFP MBH injection, after intracerebroventricular administration of vehicle or α MSH. AAV-Cre: $n=18$ (vehicle), $n=15$ (α MSH). AAV-GFP: $n=14$ (vehicle), $n=12$ (α MSH). 3V, third ventricle. Scale bars in **a, d, g, j, l**, 50 μ m. Data are mean \pm s.e.m. In **b** and **e**, $^{\&}P < 0.0001$ for comparisons of GFP-positive/Pomc-positive or GFP-positive/Pomc-negative subpopulation counts between *Pomc-Cre;Tbx3^{loxP/loxP};ROSA^{mT/mG}* mice and controls, $^{**}P = 0.0025$ for comparison between total number of Cre-recombined neurons of *Pomc-Cre;Tbx3^{loxP/loxP};ROSA^{mT/mG}* mice and controls, using ANOVA followed by Sidak's post-test. In **f** and **i**, $^{***}P = 0.0003$ and $^{**}P = 0.0071$ using two-tailed t test. In **k**, $^{*}P = 0.04$, $^{\&\&}P = 0.011$ comparing ad libitum fed *Pomc-Cre;Tbx3^{loxP/loxP};ROSA^{mT/mG}* mice vs ad libitum fed controls; $^{\&\&}P = 0.027$ comparing refed *Pomc-Cre;Tbx3^{loxP/loxP};ROSA^{mT/mG}* mice vs refed controls, by ANOVA followed by Tukey's post-test. In **m**, $^{***}P < 0.0001$ using two-tailed t test. In **n**, $^{**}P = 0.0061$ by ANOVA followed by Tukey's post-test. The experiments in **a** were repeated two independent times with similar results. The experiments in **d, g, j** were performed one time with several samples showing similar results. The experiments in **l** were repeated two independent times with similar results.

Tbx3 functions are conserved in *Drosophila* and human neurons.

The T-box family of transcription factors is remarkably conserved among species³². In *Drosophila melanogaster*, a Tbx3 homologue protein is encoded by the gene *omb* (or *bifid*). *Omb* is expressed in the CNS of adult flies, as assessed by double immunohistochemis-

try between *omb* and the synaptic marker bruchpilot (labelled by the Nc82 antibody) (Fig. 5a and Supplementary Fig. 6). To address whether neuronal Tbx3 action on energy homeostasis is conserved in *Drosophila*, we generated flies bearing an inducible nervous-system-specific *omb*-knockdown system (Fig. 5b). Relative to what occurred

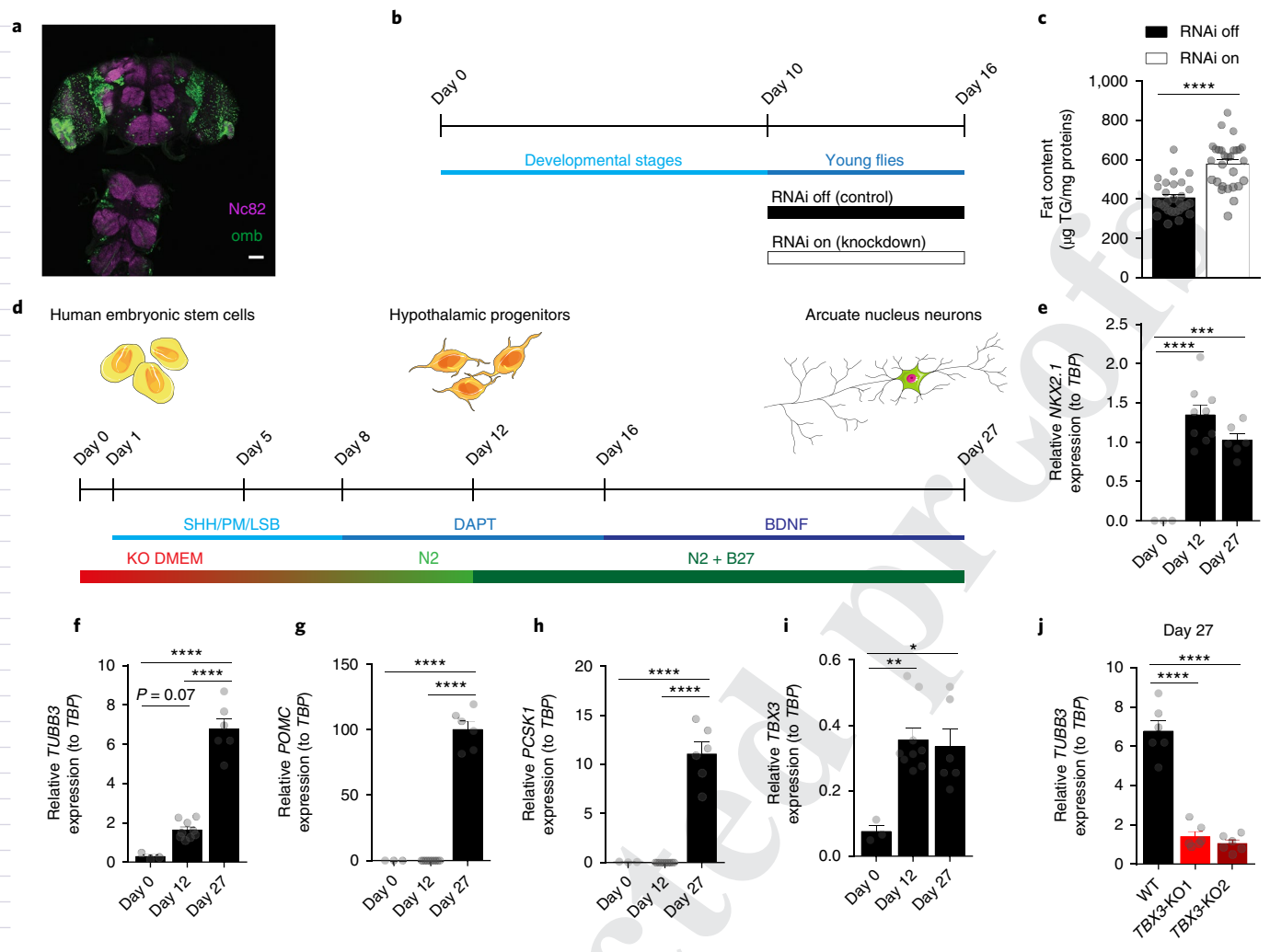


Fig. 5 | *Tbx3* functions in *Drosophila* and human neurons. **a**, Representative image depicting expression of the *Drosophila Tbx3* orthologue omb (omb expression assessed via GFP in ombP3-Gal4 > GFP flies) and Nc82 (neuronal marker) in the central nervous system of *Drosophila melanogaster*. Scale bar, 50 μ m. **b**, Timeline of RNA interference (RNAi) knockdown of *omb* (RNAi on), and control flies (RNAi off). **c**, Quantification of *Drosophila* body fat content after knockdown of *omb* (RNAi on, $n = 28$) compared with controls (RNAi off, $n = 28$) using the omb-RNAi line 1. **d**, Differentiation of human ESC into hypothalamic arcuate-like neurons. The combination of dual SMAD inhibition (L, LDN193189, 2.5 μ M; SB, SB431542, 10 μ M), early activation of sonic hedgehog (SHH) signalling (100 ng/ml SHH; SHH agonist PM, purmorphamine, 2 μ M) and step-wise switch from ESC medium (KO DMEM) to neural progenitor medium (N2) followed by inhibition of Notch signalling (DAPT, 10 μ M) converts hESC into hypothalamic progenitors. For neuronal maturation, cells are cultured in neuronal medium (N2 + B27), treated with DAPT and subsequently exposed to BDNF (brain-derived neurotrophic factor, 20 ng/ml). **e-i**, Gene expression analyses of *NKX2.1* (**e**), *TUBB3* (**f**), *POMC* (**g**), *PCSK1* (**h**), and *TBX3* (**i**) over the time course of differentiation of ESC into hypothalamic neurons by qRT-PCR. **j**, Gene expression analysis by qRT-PCR of *TUBB3* in wild-type (WT) human ESC clones and in *TBX3* knockout (*TBX3*-KO1 and *TBX3*-KO2) cell lines at ARC-like neurons (day 27) stage. Data are mean \pm s.e.m. In **e-i**, $n = 3$ (day 0), $n = 9$ (day 12), $n = 6$ (day 27). In **j**, $n = 6$ per group. In **c**, **** $P < 0.0001$ using two-tailed *t* test. In **e**, **** $P < 0.0001$ and *** $P = 0.0005$ using ANOVA followed by Tukey's post-test. In **f-i**, * $P = 0.01$, ** $P = 0.0039$ and **** $P < 0.0001$ using ANOVA followed by Tukey's post-test. In **j**, **** $P < 0.0001$ using ANOVA followed by Dunnett's post-test. The experiment in **a** was repeated two independent times with similar results.

in controls (RNAi off), knockdown of *omb* (RNAi on) induced a significant increase in body fat content (Fig. 5c). These results were reproduced in a second transgenic *Drosophila* model using a different *omb* RNAi targeted sequence (Supplementary Fig. 6).

To determine whether *Tbx3* loss-of-function phenotypes can be recapitulated in a relevant human neurocellular model system, we investigated the role of *TBX3* in the control of differentiation and the peptidergic profile of human hypothalamic neurons. H9 human embryonic stem cells (hESC; WA09; WiCell) were differentiated into ARC-like neurons over the course of 27 d (Fig. 5d), as previously described^{33–35}. In this in vitro human hypothalamic neuronal model, *NKX2.1* expression can be observed by day 12 of differentiation, corresponding to the hypothalamic progenitor stage (Fig. 5e).

Low-level expression of *class III β -tubulin* (*TUBB3*), a neuronal differentiation marker, occurs by day 12 and reaches maximum at day 27 (Fig. 5f). Expression of *POMC* and its processing enzyme *proprotein convertase subtilisin/kexin type 1* (*PCSK1*) can be detected after neuronal maturation at day 27 (Fig. 5g,h). *TBX3* expression was observed in this model at day 12 of differentiation, corresponding to the *NKX2.1*-positive hypothalamic progenitor stage, and *TBX3* levels remained stable in differentiated ARC-like neurons as obtained on day 27 (Fig. 5i).

To assess the impact of *TBX3* deletion on human hypothalamic neuronal differentiation, two independent *TBX3*-KO hESC lines were generated using CRISPR–Cas9 (Supplementary Fig. 6). Despite efficient *TBX3* ablation (Supplementary Fig. 6), no change

in hypothalamic progenitor marker *NKX2.1* was observed at day 12 in either *TBX3*-KO line (Supplementary Fig. 6), suggesting normal differentiation into hypothalamic progenitors. At day 27, *NKX2.1* as well as *TUBB3*, the marker for neuronal differentiation, were greatly reduced in *TBX3*-KO cells compared with WT cells (Supplementary Fig. 6 and Fig. 5j, respectively), indicative of an impaired neuronal maturation state in the *TBX3*-KO condition in this *in vitro* human neurocellular model system. *In silico* analysis of the genomic loci of genes coding for human POMC, CART and AGRP for potential Tbx3-binding sites (T-box binding motifs) revealed, as in mice, Tbx3-binding sites in all three genomic loci (Supplementary Fig. 6). However, since the strong reduction in *TUBB3* in the absence of *TBX3* indicates that some hypothalamic differentiation programmes are halted, further analysis of expression levels for neuropeptides such as *POMC* is precluded.

Together, these data reveal that *TBX3* is essential for the maturation of hypothalamic progenitors into ARC-like POMC-expressing neurons. Furthermore, our data suggest that Tbx3 has a conserved role in the regulation of energy homeostasis in invertebrates and mammals, including humans, albeit the molecular and cellular underpinnings might differ across different species.

Discussion

The heterogeneity of hypothalamic ARC neurons allows rapid and precise physiological adaptation to changes in body energy status and is thus highly relevant for adequate maintenance of energy homeostasis. Although several transcriptional nodes are known to establish hypothalamic neuronal identity by controlling early neurogenesis and cellular fate during embryonic life^{28,36–38}, the molecular programme driving the terminal specification and identity maintenance of ARC neurons during postnatal life remains incompletely understood, with some advances identifying *Islet-1* (refs. ^{39,40}), *Bsx*⁴¹, and miRNAs⁴² as crucial regulators.

In the present experiments, we demonstrate that the transcription factor Tbx3 is required for terminal specification of hypothalamic ARC melanocortin neurons during neonatal development and is also required for the normal maintenance and plasticity of their peptidergic programme throughout adulthood.

Our work highlights a previously uncharacterized role for Tbx3 in the regulation of energy metabolism. The brain expression profile and the functional data presented reveal that Tbx3 action in hypothalamic neurons contributes to the CNS-mediated control of systemic metabolism. Loss of Tbx3 in Pomc-expressing neurons during development causes glucose intolerance and obesity secondary to decreased energy expenditure and lipid utilization in adult mice.

These metabolic alterations are accompanied by a massive decrease in the number of Pomc-expressing neurons during postnatal life, independently from changes in the cell number, which probably underlies the observed obesity phenotype. In agreement, neonatal Pomc neuronal ablation promotes similar metabolic alterations⁴³. Intriguingly, constitutive loss of Tbx3 specifically in *Agrp*/*Npy* coexpressing neurons does not translate into phenotypic metabolic changes, albeit with a significant reduction in *Agrp* and *Npy* expression. Such lack of metabolic alterations in this model is probably the result of compensatory developmental mechanisms masking the ability of *Agrp* and *Npy* to modulate systemic metabolism⁴⁴, a phenomenon previously observed after neonatal *Agrp*/*Npy* neuronal ablation^{45,46}. Thus, Tbx3 impacts systemic energy homeostasis by controlling the peptidergic identity profile of different populations that directly modulate the activity of the melanocortin system in ARC neurons during neonatal life, when maturation of the melanocortin system occurs^{28,47}.

Importantly, *Tbx3* deletion in fully mature adult hypothalamic ARC neurons selectively reduces the number of Pomc-expressing neurons, phenocopying the observation in mice with *Pomc*-promoter-driven deletion of *Tbx3* from the genome at mid-term

developmental stages. This translates into dysregulated central melanocortin tone that is in turn linked to hyperphagia, alteration in systemic lipid oxidation capacity and obesity. All of these are in agreement with the physiological role of Pomc neurons and the central melanocortin system during adulthood^{48,49}. Thus, Tbx3 is not only required for establishing POMC identity during neonatal life, but likely plays a key role in maintaining the peptidergic identity and functional activity of fully differentiated ARC neurons.

The cellular and metabolic effects provoked by *Tbx3* ablation in hypothalamic ARC neurons are independent from neuronal survival and/or turnover, as demonstrated by our cell-lineage tracing approach. Rather, Tbx3 seems to direct intracellular programmes controlling the neuronal differentiation state, in agreement with previous studies linking Tbx3 intracellular activity with differentiation and cell fate commitment in non-neuronal cells^{9–11}. Whether Tbx3 loss-of-function in immature and/or fully differentiated hypothalamic neurons may induce cellular reprogramming and a peptidergic identity switch is a compelling hypothesis requiring further scrutiny, but it is supported by evidence of neuronal developmental plasticity within the mammalian CNS^{50–52}. In this context, our *in silico*-based prediction of Tbx3-binding sites suggests that the observed changes in the peptidergic identity profiles might also be explained by direct transcriptional effects in *Pomc*, *Cart* and *Agrp* genomic loci. However, a more comprehensive and unbiased analysis, such as by chromatin immunoprecipitation followed by high-throughput sequencing, will be required to directly test this hypothesis. Similarly, a detailed characterization of the molecular machinery controlled by Tbx3 in hypothalamic neurons will be necessary to elucidate the main intracellular mechanisms underlying the metabolic effects observed. Our profiling of genes and proteins linked with Tbx3 does not allow causally linking them with the metabolic changes observed, but this initial effort may spur future research addressing the role of such Tbx3-linked machinery in the context of obesity. It will also be of paramount importance to determine whether Tbx3 influences neuropeptidergic profiles and systemic metabolism via interactions with known metabolic signals implicated in neuronal specification, such as neurogenin 3, Mash1, OTP, or *Islet-1* (refs. ^{37–39}).

Our observations in *Drosophila melanogaster* suggest that the link between neuronal Tbx3 action and systemic energy homeostasis is probably evolutionarily conserved; however, our data do not allow us to comprehend the cellular and molecular mechanism underlying the obese-like phenotype observed in flies, nor whether these mechanisms are conserved across different species. Because *Drosophila* does not express *Pomc*, *Agrp* or any homologue peptide, another neuronal population might link Tbx3 action with adiposity regulation in this species. Intriguingly, our data show that *TBX3* is essential for the maturation of hypothalamic progenitors into ARC-like human neurons. Because human subjects with *TBX3* mutations display pathological conditions consistent with ARC neuronal dysfunction (obesity, impaired GHRH release, and alterations in reproductive capacity^{13,14}), we speculate that mutations affecting *TBX3* in humans might undermine ARC neuronal differentiation status and/or peptidergic profiles, changes that ultimately impact body weight regulation, reproduction and growth. Thus, our findings might have implications for human pathophysiology.

Neurons sensitive to the orexigenic hormone ghrelin express Tbx3, such that ghrelin may also regulate directly Tbx3 expression⁵. Moreover, we uncovered a clear link between nutritional status, Tbx3 action, and neuropeptide expression in hypothalamic Pomc neurons. Whether hormonal factors and nutritional status in turn alter the peptidergic identity of hypothalamic neurons in physiological or pathophysiological conditions via modulation of Tbx3 remains a critical question. A detailed characterization of the role of Tbx3 in the context of nutritional and hormonal-based regulation of hypothalamic neuronal activity might help in deciphering

the main environmental factors controlling peptidergic identity development, maintenance and potential plasticity in mammalian CNS neurons.

We uncovered a molecular switch implicated in the terminal differentiation of body-weight-regulating ARC neurons into specific peptidergic subtypes, unravelling one of the mechanisms responsible for the neuronal heterogeneity of hypothalamic ARC neurons. Our findings represent another step toward the identification the key molecular machinery controlling the functional identity of hypothalamic neurons, particularly during postnatal life, and this may in turn facilitate the understanding of the fundamental neuronal mechanisms implicated in the pathogenesis of obesity and its associated metabolic perturbations.

Methods

Ethical compliance statement. All animal experiments were approved and conducted under the guidelines of Helmholtz Zentrum Munich and of the Faculty Animal Committee at the University of Santiago de Compostela.

Mice. All experiments were conducted on male mice. Mice were fed a standard chow diet and group housed on a 12 h:12 h light:dark cycle at 22 °C with free access to food and water unless indicated otherwise. C57BL/6J mice were provided by Jackson Laboratories. *Tbx3^{loxP/loxP}* mice were generated previously⁵³ and backcrossed on a C57BL/6J background for five generations. *Pomc-Cre* mice (Jax mice stock # 5965, ref. ²¹) and *Agrp-Cre* mice (Jax mice stock # 012899, ref. ²⁰) were mated with *Tbx3^{loxP/loxP}* mice to generate *Pomc-* and *Agrp-*specific *Tbx3*-knockout mice (*Pomc-Cre;Tbx3^{loxP/loxP}* or *Agrp-Cre;Tbx3^{loxP/loxP}*). *Pomc-Cre;Tbx3^{loxP/loxP}* and control (*Pomc-Cre*) mice were crossed with a ROSA^{mt/mG} reporter line (Jax mice stock # 007576, ref. ⁵⁴) so that neurons that express *Pomc* are permanently marked. *Pomc-Cre;Tbx3^{loxP/loxP}*, *Agrp-Cre;Tbx3^{loxP/loxP}* or control mice (*Tbx3^{loxP/loxP}*) were crossed with mice selectively expressing the green fluorescent protein (GFP) in *Npy*-expressing neurons (*Npy-GFP*, Jax mice stock # 006417 (ref. ⁵⁵) or in *Pomc*-expressing neurons (*Pomc-GFP*, Jax mice stock # 009593, ref. ⁵⁶). The *Tbx3-Cre-Venus* mouse line was created by using CRISPR-Cas9 technology. The coding sequences for 2A peptide bridges, Cre recombinase and Venus fluorescent protein, and bovine growth hormone polyadenylation signal were cloned into a targeting vector between 5' and 3' homology arms flanking the stop codon of the *Tbx3* locus. Homologous recombination was confirmed by PCR and Southern blot analysis (using the DIG system from Roche, Indianapolis, IN). For the studies involving embryos, the breeders were mated 1 h before the dark phase and checked for a vaginal plug the next day. The day of conception (sperm-positive vaginal smear) was designated as embryonic day 0 (E0). The day of birth was considered postnatal day 0 (P0). Additional information is in the Reporting Summary.

Physiological measures. To measure food consumption, mice were housed two to three per cage. Body composition (fat and lean mass) was measured using quantitative nuclear magnetic resonance technology (EchoMRI, Houston, TX). Energy expenditure and the respiratory exchange ratio were assessed using a combined indirect calorimetry system (TSE PhenoMaster, TSE Systems, Bad Homburg, Germany). O₂ consumption and CO₂ production were measured every 10 min for a total of up to 120 h (after a minimum of 48 h of adaptation). Energy expenditure (EE, kcal/h) values were correlated to the body weight of the animals recorded at the end of the measurement using analysis of covariance (ANCOVA)¹⁹. For the analysis of glucose tolerance, mice were injected intraperitoneally with 1.75 g glucose per kg of body weight (*Agrp-Cre;Tbx3^{loxP/loxP}* mice) or 1.5 g glucose per kg of body weight (*Pomc-Cre;Tbx3^{loxP/loxP}* mice). 20% (w/v) D-glucose (Sigma-Aldrich) in 0.9% (w/v) saline was used. Tail blood glucose concentrations (mg/dl) were measured using a handheld glucometer (TheraSense Freestyle).

Viral-mediated deletion of *Tbx3*. To ablate *Tbx3* in the MBH, recombinant adeno-associated viruses (AAV) carrying the Cre recombinase and the hemagglutinin (HA)-tag (AAV-Cre) or control viruses carrying *Renilla* GFP (AAV-GFP), were generated as previously described³⁷ and injected bilaterally (0.5 μl/side; 1.0 × 10¹¹ viral genomes/ml) into the MBH of *Tbx3^{loxP/loxP}* mice (12 weeks old), using a motorized stereotaxic system from Neurostar (Tubingen, Germany). The nuclear localization signal (nls) of the simian virus 40 large T antigen and the Cre-recombinase coding region was fused downstream of the HA tag, in a rAAV plasmid backbone containing the 1.1 kb CMV immediate early enhancer/chicken β-actin hybrid promoter (CBA), the woodchuck post-transcriptional regulatory element (WPRE), and the bovine growth hormone poly(A) (bGH) to obtain rAAV-CBA-WPRE-bGH carrying Cre-recombinase (AAV-Cre). The rAAV-CBA-WPRE-bGH backbone carrying the *Renilla* GFP cDNA (Stratagene) was used as negative control. rAAV chimeric vectors (virions containing a 1:1 ratio of AAV1 and AAV2 capsid proteins with AAV2 ITRs) were generated by transfecting HEK293 cells with the AAV cis plasmid, the AAV1 and AAV2 helper plasmids, and the adenovirus helper plasmid by standard PEI transfection methods. 60 h after

transfection, cells were harvested, and the vector was purified using OPTIPREP density gradient (Sigma). Genomic titre were determined using the ABI 7700 real-time PCR cycler (Applied Biosystems) with primers designed to WPRE. Virus was injected bilaterally (0.5 μl/side; 1.0 × 10¹¹ viral genomes/ml) into the MBH of *Tbx3^{loxP/loxP}* mice (12 weeks old), using a motorized stereotaxic system from Neurostar (Tubingen, Germany). Stereotaxic coordinates were -1.6 mm posterior and ±0.25 mm lateral to bregma and -5.8 mm ventral from the dura. During the same procedure, a stainless-steel cannula (Bilaney Consultants GmbH, Düsseldorf, Germany) was implanted into the lateral cerebral ventricle. Stereotaxic coordinates for intracerebroventricular (ICV) injections were -0.8 mm posterior, -1.4 mm lateral from bregma and -2.0 mm ventral from dura. Surgeries were performed using a mixture of ketamine and xylazine (100 mg/kg and 7 mg/kg, respectively) as anaesthetic agents and Metamizol (200 mg/kg, subcutaneous), then Meloxicam (1 mg/kg, on 3 consecutive days, subcutaneous) for postoperative analgesia. For ICV studies, mice were infused with 1 μl of either vehicle (aCSF; Tocris Bioscience) or α-MSH (1 nmol, R&D systems, Tocris) 2 h before the onset of the dark cycle, and food intake followed immediately for 24 h.

BrdU experiments. 50 mg/kg of bromodeoxyuridine (BrdU) in ~50 μl of sterile saline was injected daily at postnatal days 0, 1, 2 and 3 in the dorsal neck fold of pups. The pups were euthanized at P7, and the brains were processed for immunohistochemistry.

Immunohistochemistry. Adult mice were transcardially perfused with PBS, then with 4% neutral buffered paraformaldehyde (PFA) (Fisher Scientific). Brains from embryos and pups were isolated from non-PFA-perfused animals. After dissection, brains were post-fixed for 24 h with 4% PFA, equilibrated in 30% sucrose for 24 h, and sectioned on a cryostat (Leica Biosystems) at 25 μm. Brain sections were incubated with the following primary antibodies: rabbit anti-*Pomc* precursor (Phoenix Pharmaceuticals), goat anti-*Agrp* (R&D systems, AF634), chicken anti-GFP (Acris, AP31791PU-N), goat anti-GFP (Abcam, ab6673), rabbit anti-*Npy* (Abcam, ab30914), rabbit anti-*Cart* (Phoenix Pharmaceuticals Inc. CA, USA), mouse anti-BrdU (Sigma), goat anti-*Tbx3* (A20, Santa Cruz Biotechnology), rabbit anti-*Tbx3* (A303-098A, Bethyl Laboratories), rabbit anti-cleaved caspase-3 (5A1E, Cell Signaling), goat anti-*Iba1* (Abcam ab107519), rabbit anti-GFAP (Dako, Z0334), chicken anti-vimentin (Sigma, Abcam ab24525), rabbit anti-HA tag (C29F4, Cell Signaling). Primary antibodies were incubated at a concentration of 1:500 overnight at 4 °C in 0.1 M TBS containing gelatine (0.25%) and Triton X-100 (0.5%). Sections were washed with 0.1 M TBS and incubated for 1 h at room temperature with 0.1 M TBS containing gelatine (0.25%) and Triton X-100 (0.5%), using the following secondary antibodies (1:1,000) from Jackson ImmunoResearch Laboratories: goat anti-rabbit (Alexa 647), goat anti-chicken (Alexa 488), donkey anti-goat (Alexa 488), and donkey anti-mouse (Alexa 488).

Image analysis. Images were obtained using a BZ-9000 microscope (Keyence) or a Leica SP5 confocal microscope, and automated analysis was performed using Fiji 1.0 (ImageJ) when technically feasible. Manual counts were performed blinded. When anatomically possible, neuronal cell counts were performed on several sections spanning the medial arcuate nucleus and averaged.

Gene expression analysis by qRT-PCR. Dissected tissues were immediately frozen on dry ice, and RNA was extracted using RNeasy Mini Kits (Qiagen). Whole hypothalamus was isolated and immediately frozen on dry ice. To obtain RNA from arcuate nucleus micropunches, freshly dissected whole brains were immersed in RNAlater (AM7021, ThermoFisher) for a minimum of 24 h at 4 °C. The RNAlater-immersed brains were subsequently cut coronally in 280 μm slices using a vibratome, and the arcuate nucleus was dissected from each slice using a scalpel visually aided by binoculars. RNA was extracted using RNeasy Mini Kits (Qiagen). cDNA was generated with reverse transcription QuantiTect reverse transcription kit (Qiagen). Quantitative real-time RT-PCR (qRT-PCR) was performed with a Viia 7 Real-Time PCR System (Applied Biosystems) using the following TaqMan probes (ThermoFisher scientific): *Hprt* (Mm01545399_m1), *Ppib* (Mm00478295_m1), *Npy* (Mm03048253_m1), *Pomc* (Mm00435874_m1), *Agrp* (Mm00475829_g1), *Kisspeptin* (Mm03058560_m1), *Somatostatin* (Mm0043667_m1), *Tyrosine hydroxylase* (Mm00447557_m1), *Ghrh* (Mm00439100_m1), *Tbx3* (Mm01195726_m1), *Pcsk1* (Mm00479023_m1), *Pcsk2* (Mm00500981_m1), *Pam* (Mm01293044_m1), and *Cpe* (Mm00516341_m1). Target gene expression was normalized to reference genes *Hprt* or *Ppib*. Calculations were performed by a comparative method (2^{-ΔΔCT}).

Primary murine hypothalamic cell cultures. Hypothalami were extracted from *Tbx3^{loxP/loxP}* mouse foetuses on embryonic day 14 (E14) in ice-cold calcium- and magnesium-free HBSS (Life Technologies), digested for 10 min at 37 °C with 0.05% trypsin (Life Technologies), washed three times with serum-free MEM supplemented with L-glutamine (2 mM) and glucose (25 mM) and dispersed in the same medium. Cells were plated on 12-well plates coated with poly-L-lysine (Sigma-Aldrich) at density 1.5 × 10⁶ per well in MEM supplemented with heat-inactivated 10% horse serum and 10% foetal bovine serum, 2 mM L-glutamine and glucose (25 mM) without antibiotics. On day 4, half the medium was replaced with

fresh culture medium lacking foetal bovine serum and containing 10 μ M mitotic inhibitor AraC (cytosine-1- β -D-arabinofuranoside, Sigma-Aldrich) to inhibit non-neuronal cell proliferation. On day 6, neurons were infected with a recombinant adenovirus carrying the coding sequence for the recombinase Cre (Ad5-CMV-Cre-eGFP, named Ad-Cre) to delete the loxP-flanked portion of the *Tbx3* gene, or with a control virus (Ad5-CMV-eGFP, named Ad-GFP) from Vector Development Laboratory (TX, USA). On day 7, after 12 h of incubation, virus-containing medium was removed and replaced with fresh growth medium. Neurons were further incubated for 48 h to ensure efficient recombination before performing experiments. Cell cytotoxicity was assessed using Pierce LDF Cytotoxicity Assay Kit (#88953, ThermoFisher Scientific).

ChIP-MS. For ChIP experiments followed by mass spectrometry (ChIP-MS), hypothalamic samples from 34 individual mice were pooled together, and five hypothalami at a time were homogenized in 9 ml of 1% formaldehyde in PBS for 10 min. After quenching for 5 min with 125 mM glycine, samples were washed twice with PBS. Pellets were resuspended in 1 ml of lysis buffer (0.3% SDS, 1.7% Triton, 5 mM EDTA, pH 8, 50 mM Tris, pH 8, 100 mM NaCl) and the chromatin was sonicated to an average size of 200 bp. After incubation with either a *Tbx3* antibody (A303-098A, Bethyl Laboratories Inc.) or an IgG antibody (rabbit IgG 2729S, Cell Signaling Technology), antibody-bait complexes were bound by protein G-coupled agarose beads (Cell Signaling Technology) and washed three times with wash buffer A (50 mM HEPES, pH 7.5, 140 mM NaCl, 1% Triton), once with wash buffer B (50 mM HEPES pH 7.5, 500 mM NaCl, 1% Triton) and twice with TBS. Beads were incubated for 30 min with elution buffer 1 (2 M urea, 50 mM Tris-HCl (pH 7.5), 2 mM DTT, 20 μ g/ml trypsin) followed by a second elution with elution buffer 2 (2 M urea, 50 mM Tris-HCl (pH 7.5), 10 mM chloroacetamide) for 5 min. Both eluates were combined and further incubated overnight at room temperature. Tryptic peptide mixtures were acidified with 1% TFA and desalted with Stage Tips containing three layers of C18 reverse phase material and analysed by mass spectrometry. Peptides were separated on 50-cm columns packed in-house with ReproSil-Pur C18-AQ 1.9 μ m resin (Dr Maisch GmbH). Liquid chromatography was performed on an EASY-nLC 1000 ultra-high-pressure system coupled through a nano-electrospray source to a Q-Exactive HF mass spectrometer (all from Thermo Fisher Scientific). Peptides were loaded in buffer A (0.1% formic acid) and separated by applying a non-linear gradient of 5–32% buffer B (0.1% formic acid, 80% acetonitrile) at a flow rate of 300 nl/min over 100 min. Data acquisition switched between a full scan and 15 data-dependent MS/MS scans. Full scans were acquired with target values of 3×10^6 charges in the 300–1,650 m/z range. The resolution for full-scan MS spectra was set to 60,000 with a maximum injection time of 20 ms. The 15 most abundant ions were sequentially isolated with an ion target value of 1×10^5 and an isolation window of 1.4 m/z. Fragmentation of precursor ions was performed by higher energy C-trap dissociation with a normalized collision energy of 27 eV. Resolution for HCD spectra was set to 15,000 with maximum ion injection time of 60 ms. Multiple sequencing of peptides was minimized by excluding the selected peptide candidates for 25 s. Raw mass spectrometry data were analysed with MaxQuant (version 1.5.6.7)⁵⁸ and Perseus (version 1.5.4.2) software packages. Peak lists were searched against the mouse Uniprot FASTA database (2015_08 release) combined with 262 common contaminants by the integrated Andromeda search engine⁵⁹. False discovery rate was set to 1% for both peptides (minimum length of 7 amino acids) and proteins. ‘Match between runs’ (MBR) with a maximum time difference of 0.7 min was enabled. For a gain in peptide identification, MS spectra were matched to a library of *Tbx3* ChIP MS data derived from murine neuronal progenitor cells. Relative protein amounts were determined using the MaxLFQ algorithm⁶⁰, with a minimum ratio count of two. Missing values were imputed from a normal distribution applying a width of 0.2 and a downshift of 1.8 standard deviations. Significant outliers were defined by permutation-controlled Student’s *t* test (FDR < 0.05, *s*₀ = 1) comparing triplicate ChIP-MS samples for each antibody. Additional information is in the Reporting Summary.

RNA sequencing. RNA-seq was performed in primary neurons isolated from *Tbx3*^{loxP/loxP} mice and treated with Ad-Cre or Ad-GFP viruses. Sequencing was performed in three independent neuronal isolations totalling 9 Ad-GFP-treated and 11 Ad-Cre-treated independent samples. Prior to library preparation, RNA integrity was determined with the Agilent 2100 Bioanalyzer using the RNA 6000 Nano Kit. All samples had RNA integrity number (RIN) values greater than 7. 1 μ g of total RNA per sample was used for library preparation. Library construction was performed as described in the Low Throughput protocol of the TruSeq RNA Sample Prep Guide (Illumina) in an automated manner, using the Bravo Automated Liquid Handling Platform (Agilent). cDNA libraries were assessed for quality and quantity with the Lab Chip GX (Perkin Elmer) and the Quant-iT PicoGreen dsDNA Assay Kit (Life Technologies). cDNA libraries were multiplexed and sequenced as 100 bp paired-end runs on an Illumina HiSeq2500 platform. About 8 Gb of sequence per sample were obtained. The GEM mapper⁶¹ (v 1.7.1) with modified parameter settings (mismatches = 0.04, min-decoded-strata = 2) was used for split-read alignment against the mouse genome assembly mm9 (NCBI37) and UCSC knownGene annotation. Duplicate reads were removed. To quantify the number of reads mapping to annotated genes, we used

HTSeq-count⁶² (v0.6.0). We normalized read counts to correct for possibly varying sequencing depths across samples using the R/Bioconductor package DESeq2 (ref. ⁶³) and excluded genes with low expression levels (mean read count < 25) from the analysis. We combined RNA-seq data of the three independent neuronal isolations. As the independence of the three neuronal isolations might introduce batch effects, we applied surrogate variable analysis implemented in the R package *sva*⁶⁴ to remove them. Gene expression levels between the two virus treatments were compared using DESeq2. We chose 0.001 to be the *P*-value cutoff after FDR correction (Benjamini–Hochberg). To obtain genes selectively expressed in Pomc neurons, we used the single-cell sequencing data set previously published⁷ and selected the n14 (Pomc/Ttr), n15 (Pomc/Anxa2) and n21 (Pomc/Glipr1) neuronal clusters as gene expression references. We chose all genes that had a normalized expression value above a noise level of 4.5. Additionally, we required the selected genes to be expressed in at least 10% of the 1,191 samples in our *Pomc* neuron reference. We intersected the genes differentially expressed in our *Tbx3* Ad-Cre⁶⁵ to test these genes against GO biological process terms⁶⁶. After the overrepresentation test, we excluded GO terms whose gene list overlapped the list of another term completely. All calculations were performed using R (v3.4.3).

Drosophila. The *Drosophila melanogaster* neuronal GeneSwitch Gal4 driver line (Elav-Gal4⁶⁸) was obtained from the Bloomington Drosophila Stock Center (BDSC43642). GeneSwitch drivers can be activated by progesterone steroids⁶⁷. The RNAi transgenic lines for the *Tbx3* homologue gene omb (line 1, UAS-ombRNAi-C4, line 2, UAS-ombRNAi-C1) were described in ref. ⁶⁸. Elav-Gal4⁶⁵ virgin females and 15 omb RNAi transgenic males were crossed in big-fly food vials for 24 h, and around 600 F1 embryos were seeded and kept at 25 °C for growth on standard cornmeal media (12 h:12 h light:dark cycle; 60–70% humidity). After eclosion (24 h), 50 young adult male and virgin females were fed on small fresh drug-food vials (mifepristone, 200 μ M) and control food vials (ethanol, same as mifepristone dissolved volume), respectively, for 6 d. At least eight technical replicates (5 flies each) were collected for body fat content measurement (TAG value normalized to protein value), based on the coupled-colorimetric assay (triglyceride, Pointe Scientific (T7532))⁶⁹ and bicinchoninic acid assay (protein, Pierce, Thermo Scientific; Cat. # 23225)^{70,71}. 5 adult male flies per technical replicate, 600 μ l homogenization buffer (0.05% Tween-20 in water) and 5 mm metal beads (QIAGEN, Cat. # 69989) were homogenized in 1.2 ml collecting tubes (QIAGEN, Cat. # 19560; Caps: Cat. # 19566) using a tissue lyser II (QIAGEN, 85300), and immediately incubated at 70 °C (water bath) for 5 min. The fly homogenates were spun down at 5,000 r.p.m. for 3 min. $2 \times 50 \mu$ l supernatant of each replicate, TAG standards solutions (Biomol, Cat. # Cay-10010509; 0, 5.5, 11, 22, 33, 44 μ g in 50 μ l homogenization buffer), BSA (bovine serum albumin), and protein standard samples (0, 25, 125, 250, 500, 750 mg/mL) were measured at 500 nm (for TAG) and 570 nm (for protein). The assay kit for the colorimetric assay was from Pointe Scientific (T7532). Immunostainings were carried out in 5-d-old adult male flies (omb-Gal4 > UAS-GFP transgenic line⁷²) using a method reported previously⁷³. Brains were dissected in cold PBS and fixed in 4% PFA in PBS at room temperature (RT) for 30 min. Brain tissues were incubated with 0.25% Triton X-100 in PBS (0.25% PBST) at RT for 25 min and blocked with 1% BSA & 3% normal goat serum (NGS) in 0.25% PBST for 1 h at RT with mild rotations. The following primary antibodies were used: mouse anti-Bruchpilot (nc82, 1:50) (nc82, deposited to the DSHB by Buchner, E. (DSHB Hybridoma Product nc82)), chicken anti-GFP (1:1,000) (Acris, AP31791PU-N), and rabbit anti-Omb serum (1:1,000)⁷⁴. The following secondary antibodies (Jackson ImmunoResearch Laboratories) were used: donkey anti-mouse (Alexa 568), goat anti-rabbit (Alexa 647), and goat anti-chicken (Alexa 488) were used. Secondary antibodies were incubated at RT for 2 h. After 5×10 min washing with 0.25% PBST and 1 \times overnight washing with PBS, tissues were mounted on gelatine-coated glass slides and coverslipped for image analysis. Images were obtained with Leica SP8 confocal system (20 \times air objective) and processed with Fiji 1.0 (ImageJ).

Human embryonic stem cells. The human H9 ESC line was purchased from WiCell. Cells were maintained in a humidified incubator at 37 °C on irradiated murine embryonic fibroblasts (MEFs; CF-1 MEF 4 M IRR; GLOBALSTEM) in DMEM KO medium (Cat # 10829018; ThermoFisher Scientific) supplemented with 15% KnockOut Serum Replacement (Cat # 10828028; ThermoFisher Scientific), 0.1 mM MEM non-essential amino acids (Cat # 11140050; ThermoFisher Scientific), 2 mM GlutaMAX (Cat # 35050061; ThermoFisher Scientific), 0.06 mM 2-Mercaptoethanol (Cat # 21985023; ThermoFisher Scientific), FGF-Basic (AA 1–155), (20 ng/ml media; Cat # PHG0263; ThermoFisher Scientific), and 10 mM Rock inhibitor (Cat # S1049; Selleckchem). Cells were passaged using Accutase (Cat # 00–4555–56; ThermoFisher Scientific). For CRISPR–Cas9-mediated deletion of *Tbx3*, pCas9_GFP was obtained from Addgene (Kiran Musunuru; # 44719). As previously published, the GFP was replaced by a truncated CD4 gene from the GeneArt’ CRISPR Nuclease OFF Vector (ThermoFisher Scientific) by GenScript using CloneEZ’ seamless cloning technology resulting in vector pCas9_CD4 (ref. ⁷⁵). The full vector sequence of pCas9_CD4 is given in Supplementary Table 4. The guide RNA sequence 5’-TCATGCGGAAGTCCGCGCC-3’ was obtained using Optimized CRISPR Design (MIT; <http://crispr.mit.edu/>). Cloning of the gRNA into pGS-U6-gRNA

was performed by GenScript. 800,000 human ESC were collected and mixed in nucleofection buffer (Human Stem Cell Nucleofector Kit 2; Cat # VPH-5022) with gRNA and pCas9_CD4 plasmids (2.5 µg each). Nucleofection was performed in an Amaxa Nucleofector II (Programme A-023) with the Human Stem Cell Nucleofector Kit 2 according to the manufacturer's instructions. Cells were plated on MEFs for 2 d for recovery, then transfected cells were purified using positive selection of CD4-expressing cells using human CD4 MicroBeads (Cat # 130-045-101; MS Column, Cat # 130-042-20; MACS Miltenyi Biotec) and replated at clonal density in 10 cm² tissue culture plates on MEFs. After 7–12 d, ESC colonies were picked into 96-well plates and, 4–5 d later, split 1:2 (one well for genomic DNA extraction followed by sequence analysis as described below, and one well for amplification of clones and further analysis and freezing, if indicated). For genomic DNA extraction and PCR analysis, genomic DNA was extracted using HotShot buffer following a published protocol⁷⁶. The DNA region of interest was PCR-amplified with the following primers: 5'-GAGAGCGCCGCCGCGCT-3' and 5'-GCTGCGGACTTGTCCCCGGCTGGA-3'⁷⁶. Sequences were generated by Sanger sequencing (Macrogen). Sequence analysis was performed to identify clones carrying mutations resulting in *TBX3* knockout. Positive clones were amplified, and genomic DNA was extracted using Genra Puregene Core Kit A (Qiagen). Topo TA Cloning Kit for sequencing (Cat # K457501; ThermoFisher Scientific) was used to determine zygosity of *TBX3* knockout with the following primers: 5'-CACCTTGGGGTCGTCCTCCA-3' and 5'-CGCAAGGCACAAGGACGGTCA-3'. G-band karyotyping analysis was done by Cell Line Genetics. Chromosome analysis was performed on 20 cells per cell line.

Differentiation of human ESC into arcuate-like neurons. Human ESCs were differentiated into hypothalamic arcuate-like neurons were derived from human ESC using a previously published protocol^{33–35}. H9 cells were plated on dishes coated with Matrigel (Cat # 08-774-552; ThermoFisher Scientific) dishes at a density of 100,000 cells/cm² in human ESC medium, as described above, supplemented with bFGF and Rock inhibitor. Cell density was observed after 24 h. If the cells were not yet at 100% confluency, medium was aspirated and replaced with ESC medium with bFGF and Rock inhibitor for another 24 h. Once cells reached 100% confluency, differentiation was initiated. 10 µM SB 431542 (Cat # S1067; Selleckchem) and 2.5 µM LDN 193189 (Cat # S2618; Selleckchem) were used from day 1 to day 8 to inhibit TGFβ and BMP signalling in order to promote neuronal differentiation from human ES cells⁷⁷. 100 ng/ml SHH (Cat # 248-BD; R&D Systems) and 2 µM purmorphamine (PM; Cat # S3042; Selleckchem) were added from days 1–8 to induce ventral brain development and NKX2.1 expression. Cells were cultured on days 1–4 in ESC medium, from days 5–8 the medium was switched stepwise from ESC medium to N2 medium (3:1, 1:1, 1:3). N2 medium (500 ml) consists of 485 ml DMEM/F12 (Cat # 11322; ThermoFisher Scientific) supplemented with 5 ml MEM non-essential amino acids (Cat # 11140050; ThermoFisher Scientific), 5 ml of a 16 % glucose solution and 5 ml N2 (Cat # 1370701; ThermoFisher Scientific). Ascorbic acid (Cat # A0278; Sigma-Aldrich) was added at just prior use at a final concentration of 200 nM. From Day 9 on cells were cultured in N2-B27 medium consisting of 475 ml DMEM/F12 (Cat # 11322; ThermoFisher Scientific) supplemented with 5 ml MEM Non-Essential Amino Acids (Cat # 11140050; ThermoFisher Scientific), 5 ml of a 16 % glucose solution, 5 ml N2 (Cat # 1370701; ThermoFisher Scientific) and 10 ml B27 (Cat # 12587010; ThermoFisher Scientific). Ascorbic acid (Cat # A0278; Sigma-Aldrich) was added at just prior use at a final concentration of 200 nM. Inhibition of Notch signalling by 10 µM DAPT (Cat # S2215; Selleckchem) was performed from Days 9 to 12. Nkx2.1+ progenitors were collected and re-plated on extracellular matrix (poly-L-ornithine [Cat # A-004-C; Millipore] and laminin [Cat # 23017015; ThermoFisher Scientific]) to enhance the attachment and differentiation of neuron progenitors. The Notch inhibitor DAPT was used to inhibit the proliferation of progenitor cells and promote further neuronal differentiation^{78,79}. The neurotrophic factor BDNF (20 ng/ml; Cat # 450-02; PeproTech) was introduced following DAPT treatment to improve the survival, differentiation and maturation of these neurons. For RT-PCR analyses, Cells at day 0, day 12 and day 27 of differentiation were homogenized in Trizol Reagent (Cat # 15596026; ThermoFisher Scientific) and total RNA was extracted using RNeasy Plus Micro Kit (Cat # 74034; Qiagen) with on-column DNaseI (Cat # 79254; Qiagen) treatment to remove genomic DNA contamination and stored at -80 °C until further processing. A total of 500 ng of total RNA was used for reverse transcription utilizing the Transcriptor First Strand cDNA Synthesis Kit (Cat # 04897030001; Roche Diagnostic, Indianapolis, IN) using a mixture of anchored oligo(dT)₁₈ and random hexamer primers according to the manufacturer's instructions. Quantitative PCR was performed with a Light-Cycler 480 (Roche Diagnostics) using SYBR Green in a total volume of 10 µl with 1 µl of template, 1 µl of forward and reverse primers (10 µM) and 5 µl of SYBR Green I Master-Mix (Cat # 04707516001; Roche Diagnostic). Reactions included an initial cycle at 95 °C for 10 min, followed by 40 cycles of denaturation at 95 °C for 10 sec, annealing at 60 °C for 5 sec, and extension at 72 °C for 15 sec. Crossing points were determined by Light-Cycler 480 software using the second derivative maximum technique. Relative expression data were calculated by the delta-delta Ct method, with normalization of the raw data to *TBP*. Quantitative PCR was performed to determine the mRNA level of *TBX3*, *POMC*, *TUBB3*, *PCSK1*, *NKX2.1*. Primer sequences are shown in Supplementary Table 1.

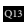
Western blot analysis. Human ESC (H9) and hypothalamic arcuate-like neurons (day 27 of differentiation) were washed with DPBS and lysed in RIPA Lysis and Extraction Buffer (Cat # 89900; ThermoFisher Scientific) with protease and phosphatase inhibitors (Cat # 78442; ThermoFisher Scientific), incubated at 4 °C for 15 min and then centrifuged at 12,000 r.p.m. for 15 min at 4 °C. 15 µg of total protein from each extract was loaded on a 4–12% gradient Bis-Tris gel (Cat # NP0335BOX; ThermoFisher Scientific) and transferred onto nitrocellulose membrane using iBlot 2 Dry Blotting System (ThermoFisher Scientific). The membrane was blocked for 1 h at room temperature with SuperBlock T20 (TBS) Blocking Buffer (Cat # 37536; ThermoFisher Scientific) and then incubated with primary antibody against *TBX3* (1:100; Cat # ab99302; Abcam) overnight at 4 °C, washed three times using TBS with 0.1% Tween-20 (Cat # 1706531; Bio-Rad), and incubated with secondary antibody anti-rabbit HRP (1:10,000; Cat # 7074 S; Cell Signaling) for 1 h at room temperature. Specific bands were then detected by electrochemiluminescence analysis using SuperSigna West Pico PLUS Chemiluminescent Substrate (Cat # 34577; ThermoFisher Scientific). An antibody against beta-actin (1:1,000; Cat # ab8226; Abcam), using anti-mouse HRP (1:10,000; Cat # 7076 S; Cell Signaling) as a secondary antibody, was used as loading control. Validation of the goat anti-Tbx3 antibody (A20, Santa Cruz Biotechnology) was performed using *Tbx3*-deficient embryos (E13.5) kindly provided by A. Kispert⁸⁰. Proteins were extracted using RIPA buffer containing protease and phosphatase inhibitor cocktail (Thermo Fisher Scientific Inc., Rockford, IL USA) 1 mM phenyl-methane-sulfonyl fluoride (PMSF) and 1 mM sodium butyrate (Sigma-Aldrich, St Louis, MO, USA). Proteins were transferred on nitrocellulose membranes using a Trans Blot Turbo transfer apparatus (Biorad, Hercules, CA, USA), stained with primary antibody goat anti-Tbx3 (1.500) and a secondary antibody anti-goat HRP (1.1000). Detection was carried out on a LiCor Odyssey instrument (Lincoln, NE, USA, software Image studio 2.0), using electrochemiluminescence (Amersham Biosciences, Piscataway, NJ, USA). Additional information available in the Reporting Summary.

Tbx3-focused single-cell RNA-sequencing analysis. Data for the scRNA-seq analysis were obtained from GEO accession codes GSE90806 and GSE93374 (ref. 7). The data matrix comprised of 21,086 cells and 22,802 genes generated from the Arcuate-median eminence (Arc-ME) of the mouse hypothalamus by Campbell et al.⁷. We used Seurat software⁸¹ to perform clustering analysis. We identified the 2,250 most-variable genes across the entire dataset controlling for the known relationship between mean expression and variance. After scaling and centring the data along each variable gene, we performed principal component analysis, and identified 25 significant PCs for downstream analysis that were used to identify 20 clusters. Similar to those identified by Campbell et al.⁷, we identified a total of 13,079 neurons and 8,007 non-neuronal cells. We further used the neuronal identities assigned by the authors for clustering the neurons into their respective neuronal clusters. For differential expression between cell type clusters, we used the negative binomial test, a likelihood ratio test assuming an underlying negative binomial distribution for UMI-based datasets.

Statistics. Statistical analyses were conducted using GraphPad Prism (version 5.0a). For each experiment, slides were numerically coded to obscure the treatment group. Statistical significance was determined using unpaired 2-tailed Student's *t* test, 1-way ANOVA or 2-way ANOVA followed by an appropriate post hoc test, as indicated in figure legends, and linear regression when appropriate. $P \leq 0.05$ was considered statistically significant. Additional information is provided in the Reporting Summary.

Reporting Summary. Further information on experimental design is available in the Nature Research Reporting Summary linked to this article.

Data availability

The authors declare that all data supporting the findings of this study are available within the paper and its supplementary information files. The RNA-seq database generated in our paper has been made publicly available through the Gene Expression Omnibus (GEO accession number: GSE119883). 

Received: 14 June 2018; Accepted: 13 December 2018;

References

1. Cone, R. D. Anatomy and regulation of the central melanocortin system. *Nat. Neurosci.* **8**, 571–578 (2005).
2. Gaulton, L., Elmquist, J. K. & Williams, K. W. Neural control of energy balance: translating circuits to therapies. *Cell* **161**, 133–145 (2015).
3. Koch, M. & Horvath, T. L. Molecular and cellular regulation of hypothalamic melanocortin neurons controlling food intake and energy metabolism. *Mol. Psychiatry* **19**, 752–761 (2014).
4. Morton, G. J., Meek, T. H. & Schwartz, M. W. Neurobiology of food intake in health and disease. *Nat. Rev. Neurosci.* **15**, 367–378 (2014).

- 790 5. Knight, Z. A. et al. Molecular profiling of activated neurons by
791 phosphorylated ribosome capture. *Cell* **151**, 1126–1137 (2012).
- 792 6. Allison, M. B. et al. TRAP-seq defines markers for novel populations of
793 hypothalamic and brainstem LepRb neurons. *Mol. Metab.* **4**, 299–309 (2015).
- 794 7. Campbell, J. N. et al. A molecular census of arcuate hypothalamus and
795 median eminence cell types. *Nat. Neurosci.* **20**, 484–496 (2017).
- 796 8. Wansleben, S., Peres, J., Hare, S., Goding, C. R. & Prince, S. T-box
797 transcription factors in cancer biology. *Biochim. Biophys. Acta* **1846**,
798 380–391 (2014).
- 799 9. Ang, L. T. et al. A roadmap for human liver differentiation from pluripotent
800 stem cells. *Cell Rep.* **22**, 2190–2205 (2018).
- 801 10. Suzuki, A., Sekiya, S., Büscher, D., Izpisúa Belmonte, J. C. & Taniguchi, H.
802 Tbx3 controls the fate of hepatic progenitor cells in liver development by
803 suppressing p19ARF expression. *Development* **135**, 1589–1595 (2008).
- 804 11. Weidgang, C. E. et al. TBX3 Directs cell-fate decision toward mesoderm.
805 *Stem Cell Rep.* **1**, 248–265 (2013).
- 806 12. Eriksson, K. S. & Mignot, E. T-box 3 is expressed in the adult mouse
807 hypothalamus and medulla. *Brain Res.* **1302**, 233–239 (2009).
- 808 13. Linden, H., Williams, R., King, J., Blair, E. & Kini, U. Ulnar Mammary
809 syndrome and TBX3: expanding the phenotype. *Am. J. Med. Genet. A* **149A**,
810 2809–2812 (2009).
- 811 14. Schinzel, A. The ulnar-mammary syndrome: an autosomal dominant
812 pleiotropic gene. *Clin. Genet.* **32**, 160–168 (1987).
- 813 15. Grill, H. J. & Hayes, M. R. Hindbrain neurons as an essential hub in the
814 neuroanatomically distributed control of energy balance. *Cell. Metab.* **16**,
815 296–309 (2012).
- 816 16. Joly-Amado, A. et al. The hypothalamic arcuate nucleus and the control
817 of peripheral substrates. *Best Pract. Res. Clin. Endocrinol. Metab.* **28**,
818 725–737 (2014).
- 819 17. Clasadonte, J. & Prevot, V. The special relationship: glia-neuron
820 interactions in the neuroendocrine hypothalamus. *Nat. Rev. Endocrinol.* **14**,
821 25–44 (2018).
- 822 18. Pontecorvi, M., Goding, C. R., Richardson, W. D. & Kessar, N. Expression
823 of Tbx2 and Tbx3 in the developing hypothalamic-pituitary axis. *Gene Expr.*
824 *Patterns* **8**, 411–417 (2008).
- 825 19. Tschöp, M. H. et al. A guide to analysis of mouse energy metabolism.
826 *Nat. Methods* **9**, 57–63 (2011).
- 827 20. Tong, Q., Ye, C.-P., Jones, J. E., Elmquist, J. K. & Lowell, B. B. Synaptic release
828 of GABA by AgRP neurons is required for normal regulation of energy
829 balance. *Nat. Neurosci.* **11**, 998–1000 (2008).
- 830 21. Balthasar, N. et al. Leptin receptor signaling in POMC neurons is required
831 for normal body weight homeostasis. *Neuron* **42**, 983–991 (2004).
- 832 22. P. P. K. et al. Coordinated control of senescence by lncRNA and a novel
833 T-box3 co-repressor complex. *eLife Sci.* **3**, e02805 (2014).
- 834 23. Coll, M., Seidman, J. G. & Müller, C. W. Structure of the DNA-bound T-box
835 domain of human TBX3, a transcription factor responsible for ulnar-
836 mammary syndrome. *Structure* **10**, 343–356 (2002).
- 837 24. Hein, M. Y. et al. A human interactome in three quantitative dimensions
838 organized by stoichiometries and abundances. *Cell* **163**, 712–723 (2015).
- 839 25. Rolland, T. et al. A proteome-scale map of the human interactome network.
840 *Cell* **159**, 1212–1226 (2014).
- 841 26. Bandyopadhyay, S. et al. A human map kinase interactome. *Nat. Methods* **7**,
842 801–805 (2010).
- 843 27. Padilla, S. L., Carmody, J. S. & Zeltser, L. M. Pomc-expressing progenitors
844 give rise to antagonistic neuronal populations in hypothalamic feeding
845 circuits. *Nat. Med.* **16**, 403–405 (2010).
- 846 28. Toda, C., Santoro, A., Kim, J. D. & Diano, S. POMC Neurons: from birth to
847 death. *Annu. Rev. Physiol.* **79**, 209–236 (2017).
- 848 29. Hahn, T. M., Breininger, J. F., Baskin, D. G. & Schwartz, M. W. Coexpression
849 of AgRP and NPY in fasting-activated hypothalamic neurons. *Nat. Neurosci.* **1**,
850 271–272 (1998).
- 851 30. Sousa-Ferreira, L., de Almeida, L. P. & Cavadas, C. Role of hypothalamic
852 neurogenesis in feeding regulation. *Trends Endocrinol. Metab.* **25**, 80–88
853 (2014).
- 854 31. Mizuno, T. M. et al. Hypothalamic pro-opiomelanocortin mRNA is reduced by
855 fasting in ob/ob and db/db mice, but is stimulated by leptin. *Diabetes* **47**,
294–297 (1998).
32. Wilson, V. & Conlon, F. L. The T-box family. *Genome Biol.* **3**, REVIEWS3008
(2002).
33. Wang, L. et al. Differentiation of hypothalamic-like neurons from human
pluripotent stem cells. *J. Clin. Invest.* **125**, 796–808 (2015).
34. Wang, L., Egli, D. & Leibel, R. L. Efficient generation of hypothalamic
neurons from human pluripotent stem cells. *Curr. Protoc. Hum. Genet.* **90**,
21.5.1–21.5.14 (2016).
35. Wang, L. et al. PC1/3 deficiency impacts pro-opiomelanocortin processing in
human embryonic stem cell-derived hypothalamic neurons. *Stem Cell Rep.* **8**,
264–277 (2017).
36. Coupe, B. & Bouret, S. G. Development of the hypothalamic melanocortin
system. *Front Endocrinol. (Lausanne)* **4**, 38 (2013).
37. Pelling, M. et al. Differential requirements for neurogenin 3 in the
development of POMC and NPY neurons in the hypothalamus. *Dev. Biol.*
349, 406–416 (2011).
38. Lee, B. et al. Dlx1/2 and Otp coordinate the production of hypothalamic
GHRH- and AgRP-neurons. *Nat. Commun.* **9**, 2026 (2018).
39. Nasif, S. et al. Islet 1 specifies the identity of hypothalamic melanocortin
neurons and is critical for normal food intake and adiposity in adulthood.
Proc. Natl Acad. Sci. USA **112**, E1861–E1870 (2015).
40. Lee, B., Lee, S., Lee, S.-K. & Lee, J. W. The LIM-homeobox transcription
factor Isl1 plays crucial roles in the development of multiple arcuate nucleus
neurons. *Development* **143**, 3763–3773 (2016).
41. Sakkou, M. et al. A role for brain-specific homeobox factor Bsx in the control
of hyperphagia and locomotory behavior. *Cell Metab.* **5**, 450–463 (2007).
42. Messina, A. et al. A microRNA switch regulates the rise in hypothalamic
GnRH production before puberty. *Nat. Neurosci.* **19**, 835–844 (2016).
43. Greenman, Y. et al. Postnatal ablation of POMC neurons induces an obese
phenotype characterized by decreased food intake and enhanced anxiety-like
behavior. *Mol. Endocrinol.* **27**, 1091–1102 (2013).
44. Morton, G. J. & Schwartz, M. W. The NPY/AgRP neuron and energy
homeostasis. *Int. J. Obes. Relat. Metab. Disord.* **25**(Suppl 5), S56–S62 (2001).
45. Luquet, S., Perez, F. A., Hnasko, T. S. & Palmiter, R. D. NPY/AgRP Neurons
are essential for feeding in adult mice but can be ablated in neonates. *Science*
310, 683–685 (2005).
46. Tan, K., Knight, Z. A. & Friedman, J. M. Ablation of AgRP neurons impairs
adaption to restricted feeding. *Mol. Metab.* **3**, 694–704 (2014).
47. Bouret, S. G. & Simerly, R. B. Minireview: leptin and development of
hypothalamic feeding circuits. *Endocrinology* **145**, 2621–2626 (2004).
48. Zhan, C. et al. Acute and long-term suppression of feeding behavior by pomc
neurons in the brainstem and hypothalamus, respectively. *J. Neurosci.* **33**,
3624–3632 (2013).
49. Nogueiras, R. et al. The central melanocortin system directly controls
peripheral lipid metabolism. *J. Clin. Invest.* **117**, 3475–3488 (2007).
50. Burbridge, S., Stewart, I. & Placzek, M. Development of the neuroendocrine
hypothalamus. *Compr. Physiol.* **6**, 623–643 (2016).
51. Dulcis, D., Jamshidi, P., Leutgeb, S. & Spitzer, N. C. Neurotransmitter
switching in the adult brain regulates behavior. *Science* **340**, 449–453 (2013).
52. Gascón, S., Masserdotti, G., Russo, G. L. & Götz, M. Direct neuronal
reprogramming: achievements, hurdles, and new roads to success. *Cell Stem
Cell* **21**, 18–34 (2017).
53. Frank, D. U., Emechebe, U., Thomas, K. R. & Moon, A. M. Mouse Tbx3
mutants suggest novel molecular mechanisms for ulnar-mammary syndrome.
PLoS One **8**, e67841 (2013).
54. Muzumdar, M. D., Tasic, B., Miyamichi, K., Li, L. & Luo, L. A global
double-fluorescent Cre reporter mouse. *Genesis* **45**, 593–605 (2007).
55. van den Pol, A. N. et al. Neuromedin B and gastrin-releasing peptide excite
arcuate nucleus neuropeptide Y neurons in a novel transgenic mouse
expressing strong Renilla green fluorescent protein in NPY neurons. *J.
Neurosci.* **29**, 4622–4639 (2009).
56. Cowley, M. A. et al. Leptin activates anorexigenic POMC neurons through a
neural network in the arcuate nucleus. *Nature* **411**, 480–484 (2001).
57. Monory, K. et al. The endocannabinoid system controls key epileptogenic
circuits in the hippocampus. *Neuron* **51**, 455–466 (2006).
58. Cox, J. & Mann, M. MaxQuant enables high peptide identification rates,
individualized p.p.b.-range mass accuracies and proteome-wide protein
quantification. *Nat. Biotechnol.* **26**, 1367–1372 (2008).
59. Cox, J. et al. Andromeda: a peptide search engine integrated into the
MaxQuant environment. *J. Proteome Res.* **10**, 1794–1805 (2011).
60. Cox, J. et al. Accurate proteome-wide label-free quantification by delayed
normalization and maximal peptide ratio extraction, termed MaxLFQ. *Mol.
Cell Proteom.* **13**, 2513–2526 (2014).
61. Marco-Sola, S., Sammeth, M., Guigó, R. & Ribeca, P. The GEM mapper: fast,
accurate and versatile alignment by filtration. *Nat. Meth.* **9**, 1185–1188 (2012).
62. Anders, S., Pyl, P. T. & Huber, W. HTSeq—a Python framework to work with
high-throughput sequencing data. *Bioinformatics* **31**, 166–169 (2015).
63. Love, M. I., Huber, W. & Anders, S. Moderated estimation of fold change and
dispersion for RNA-seq data with DESeq2. *Genome Biol.* **15**, 550 (2014).
64. Leek, J. T. & Storey, J. D. Capturing heterogeneity in gene expression studies
by surrogate variable analysis. *PLoS Genet.* **3**, e161 (2007).
65. Yu, G., Wang, L.-G., Han, Y. & He, Q.-Y. clusterProfiler: an R package
for comparing biological themes among gene clusters. *OMICS* **16**,
284–287 (2012).
66. Ashburner, M. et al. Gene ontology: tool for the unification of biology. the
gene ontology consortium. *Nat. Genet.* **25**, 25–29 (2000).
67. Osterwalder, T., Yoon, K. S., White, B. H. & Keshishian, H. A conditional
tissue-specific transgene expression system using inducible GAL4. *Proc. Natl
Acad. Sci. USA* **98**, 12596–12601 (2001).
68. Shen, J., Dorner, C., Bahlo, A. & Pflugfelder, G. O. optomotor-blind
suppresses instability at the A/P compartment boundary of the Drosophila
wing. *Mech. Dev.* **125**, 233–246 (2008).

- 856 69. Hildebrandt, A., Bickmeyer, I. & Kühnlein, R. P. Reliable Drosophila
857 body fat quantification by a coupled colorimetric assay. *PLoS One* **6**,
858 e23796 (2011).
- 859 70. Gálíková, M., Klepsatel, P., Xu, Y. & Kühnlein, R. P. The obesity-related
860 adipokinetic hormone controls feeding and expression of neuropeptide
861 regulators of Drosophila metabolism. *Eur. J. Lipid Sci. Tech.* **119**,
862 1600138 (2017).
- 863 71. Klepsatel, P., Gálíková, M., Xu, Y. & Kühnlein, R. P. Thermal stress depletes
864 energy reserves in Drosophila. *Sci. Rep.* **6**, 33667 (2016).
- 865 72. Mayer, L. R., Diegelmann, S., Abassi, Y., Eichinger, F. & Pflugfelder, G. O.
866 Enhancer trap infidelity in Drosophila optomotor-blind. *Fly* **7**,
867 118–128 (2013).
- 868 73. Baumbach, J., Xu, Y., Hehlert, P. & Kühnlein, R. P. $G\alpha_q$, $G\gamma 1$ and $Plc21C$
869 control Drosophila body fat storage. *J. Genet. Genom.* **41**, 283–292 (2014).
- 870 74. Shen, J., Dahmann, C. & Pflugfelder, G. O. Spatial discontinuity of
871 optomotor-blind expression in the Drosophila wing imaginal disc disrupts
872 epithelial architecture and promotes cell sorting. *BMC Dev. Biol.* **10**,
873 23 (2010).
- 874 75. Stratigopoulos, G., De Rosa, M. C., LeDuc, C. A., Leibel, R. L. & Doege, C.
875 A. DMSO increases efficiency of genome editing at two non-coding loci.
876 *PLoS One* **13**, e0198637 (2018).
- 877 76. Santos, D. P., Kiskinis, E., Eggan, K. & Merkle, F. T. Comprehensive protocols
878 for crispr/cas9-based gene editing in human pluripotent stem cells. *Curr.*
879 *Protoc. Stem Cell Biol.* **38**, 5B.6.1–5B.6.60 (2016).
- 880 77. Chambers, S. M. et al. Highly efficient neural conversion of human ES
881 and iPS cells by dual inhibition of SMAD signaling. *Nat. Biotechnol.* **27**,
882 275–280 (2009).
- 883 78. Crawford, T. Q. & Roelink, H. The notch response inhibitor DAPT
884 enhances neuronal differentiation in embryonic stem cell-derived embryoid
885 bodies independently of sonic hedgehog signaling. *Dev. Dyn.* **236**,
886 886–892 (2007).
- 887 79. Nelson, B. R., Hartman, B. H., Georgi, S. A., Lan, M. S. & Reh, T. A.
888 Transient inactivation of Notch signaling synchronizes differentiation of
889 neural progenitor cells. *Dev. Biol.* **304**, 479–498 (2007).
80. Trowe, M.-O. et al. Inhibition of Sox2-dependent activation of Shh in the
ventral diencephalon by Tbx3 is required for formation of the
neurohypophysis. *Development* **140**, 2299–2309 (2013).
81. Satija, R., Farrell, J. A., Gennert, D., Schier, A. F. & Regev, A. Spatial
reconstruction of single-cell gene expression data. *Nat. Biotechnol.* **33**,
495–502 (2015).

Acknowledgements

We thank A. Kispert and M.-O. Trowe for kindly providing Tbx3-deficient embryos, J. Friedman for scientific guidance and for graciously providing access to data shown in ref. 3, M. Guzmán for assistance with the generation of AAV-GFP and AAV-Cre viral particles, the Bloomington Drosophila Stock Center (BDSC) (NIH P40OD018537) for fly stocks, and C. Layritz, H. Hoffmann, N. Wiegert and C. L. Holleman for technical assistance and assistance with animal studies. A.F. holds a postdoctoral fellowship from the Canadian Institutes of Health Research (Funding reference number: 152588). V.V.T. is supported by NIH-NIDDK grant 5K23DK110539 and in part by the Baylor-Hopkins Center for Mendelian Genomics through NHGRI grant 5U54HG006542. C.A.D. is supported by funding from the NIH (R01 DK52431, R01 DK110113 and P30 DK26687) and Columbia Stem Cell Initiative Seed Fund Program. We thank the Fondation Recherche Medicale (ARF20140129235, L.B.). This work was strongly supported by the Helmholtz Alliance ICEMED & the Helmholtz Initiative on Personalized Medicine iMed by Helmholtz Association. This work was supported in part by the Helmholtz cross-program topic “Metabolic Dysfunction”, the European Research Council ERC (AdG HypoFlam no. 695054) and in part by funding to M.H.T., Y.L., B.L. and V.K. from the Alexander von Humboldt Foundation.

Author contributions

C.Q. and A.F. designed and performed the experiments and interpreted the data. Y.X., G.C., B.L. Y.-T.T., A.R., M.W., M.C.D., V.K., R.R., V.V.T., E.G., T.M.S., A.-L.P., T.G., O.L., A.C.-S., D.K., L.B., S.C.W., G.O.P., R.N., L.Z., I.C.G.K., A.M., C.G.-C., M.M., M.T., C.A.D. performed experiments and/or edited the manuscript. M.H.T. conceptualized the project, interpreted the data, and cowrote the manuscript together with C.Q. and A.F.

Competing interests

The authors declare no competing interests.

Additional information

Supplementary information is available for this paper at <https://doi.org/10.1038/s42255-018-0028-1>.

Reprints and permissions information is available at www.nature.com/reprints.

Correspondence and requests for materials should be addressed to M.H.T.

Publisher's note: Springer Nature remains neutral with regard to jurisdictional claims in published maps and institutional affiliations.

© The Author(s), under exclusive licence to Springer Nature Limited 2019

QUERY FORM

Nature Metabolism	
Manuscript ID	[Art. Id: 28]
Author	Carmelo Quarta

AUTHOR:

The following queries have arisen during the editing of your manuscript. Please answer by making the requisite corrections directly in the e-proofing tool rather than marking them up on the PDF. This will ensure that your corrections are incorporated accurately and that your paper is published as quickly as possible.

Query No.	Nature of Query
Q1:	Please ensure that genes are correctly distinguished from gene products: for genes, official gene symbols (e.g., NCBI Gene) for the relevant species should be used and italicized; gene products such as proteins and noncoding RNAs should not be italicized.
Q2:	Please clarify whether the splitting of the original affiliations 3,12,14,17 as done is correct. If not, please indicate how they should be sorted out.
Q3:	Please check your article carefully, coordinate with any co-authors and enter all final edits clearly in the eproof, remembering to save frequently. Once corrections are submitted, we cannot routinely make further changes to the article.
Q4:	Note that the eproof should be amended in only one browser window at any one time; otherwise changes will be overwritten.
Q5:	Author surnames have been highlighted. Please check these carefully and adjust if the first name or surname is marked up incorrectly. Note that changes here will affect indexing of your article in public repositories such as PubMed. Also, carefully check the spelling and numbering of all author names and affiliations, and the corresponding email address(es).
Q6:	Please note that after the paper has been formally accepted you can only provide amended Supplementary Information files for critical changes to the scientific content, not for style. You should clearly explain what changes have been made if you do resupply any such files.
Q7:	Your paper has been copy edited. Please review every sentence to ensure that it conveys your intended meaning; if changes are required, please provide further clarification rather than reverting to the original text. Please note that formatting (including hyphenation, Latin words, and any reference citations that might be mistaken for exponents) has been made consistent with our house style.
Q8:	Please define NTS at first mention.
Q9:	Please provide catalog number for anti-Pomc precursor antibody.
Q10:	Please defined TBS at first mention.
Q11:	Please include affiliation institutions for those who supplied reagents, mice, etc.
Q12:	Please check that all funders have been appropriately acknowledged and that all grant numbers are correct.

QUERY FORM

Nature Metabolism	
Manuscript ID	[Art. Id: 28]
Author	Carmelo Quarta

AUTHOR:

The following queries have arisen during the editing of your manuscript. Please answer by making the requisite corrections directly in the e-proofing tool rather than marking them up on the PDF. This will ensure that your corrections are incorporated accurately and that your paper is published as quickly as possible.

<i>Query No.</i>	<i>Nature of Query</i>
Q13:	If applicable, please ensure accession codes are scheduled for release on or before this article's scheduled publication date, and update the database record with publication details from this article once available.
Q14:	Please check that the Competing Interests declaration is correct as stated. If you declare competing interests, please check the full text of the declaration for accuracy and completeness.

Reporting Summary

Nature Research wishes to improve the reproducibility of the work that we publish. This form provides structure for consistency and transparency in reporting. For further information on Nature Research policies, see [Authors & Referees](#) and the [Editorial Policy Checklist](#).

Statistical parameters

When statistical analyses are reported, confirm that the following items are present in the relevant location (e.g. figure legend, table legend, main text, or Methods section).

n/a Confirmed

- The exact sample size (n) for each experimental group/condition, given as a discrete number and unit of measurement
- An indication of whether measurements were taken from distinct samples or whether the same sample was measured repeatedly
- The statistical test(s) used AND whether they are one- or two-sided
Only common tests should be described solely by name; describe more complex techniques in the Methods section.
- A description of all covariates tested
- A description of any assumptions or corrections, such as tests of normality and adjustment for multiple comparisons
- A full description of the statistics including central tendency (e.g. means) or other basic estimates (e.g. regression coefficient) AND variation (e.g. standard deviation) or associated estimates of uncertainty (e.g. confidence intervals)
- For null hypothesis testing, the test statistic (e.g. F , t , r) with confidence intervals, effect sizes, degrees of freedom and P value noted
Give P values as exact values whenever suitable.
- For Bayesian analysis, information on the choice of priors and Markov chain Monte Carlo settings
- For hierarchical and complex designs, identification of the appropriate level for tests and full reporting of outcomes
- Estimates of effect sizes (e.g. Cohen's d , Pearson's r), indicating how they were calculated
- Clearly defined error bars
State explicitly what error bars represent (e.g. SD, SE, CI)

Our web collection on [statistics for biologists](#) may be useful.

Software and code

Policy information about [availability of computer code](#)

Data collection

SOFTWARES USED FOR DATA COLLECTION INCLUDE: Light-Cycler 480 version 1.5, LiCor Image studio 2.0

Data analysis

DATA WAS ANALYZED USING: GraphPad Prism 5, ImageJ (Fiji), MaxQuant (version 1.5.6.7), Perseus (version 1.5.4.2) software packages, Seurat software (Satija et al., Nat. Biotechnol. 33, 495–502 (2015))

For manuscripts utilizing custom algorithms or software that are central to the research but not yet described in published literature, software must be made available to editors/reviewers upon request. We strongly encourage code deposition in a community repository (e.g. GitHub). See the Nature Research [guidelines for submitting code & software](#) for further information.

Data

Policy information about [availability of data](#)

All manuscripts must include a [data availability statement](#). This statement should provide the following information, where applicable:

- Accession codes, unique identifiers, or web links for publicly available datasets
- A list of figures that have associated raw data
- A description of any restrictions on data availability

Data for the scRNA-seq analysis were obtained from GEO Accession codes GSE90806 and GSE93374. The RNA-seq database generated in our paper has been made publicly available: GEO accession number: GSE119883. Raw data for Supplementary Figure 3G is provided as a separate Excel file.

Field-specific reporting

Please select the best fit for your research. If you are not sure, read the appropriate sections before making your selection.

Life sciences Behavioural & social sciences Ecological, evolutionary & environmental sciences

For a reference copy of the document with all sections, see [nature.com/authors/policies/ReportingSummary-flat.pdf](https://www.nature.com/authors/policies/ReportingSummary-flat.pdf)

Life sciences study design

All studies must disclose on these points even when the disclosure is negative.

Sample size	We did not specifically perform a sample size calculation for most of studies as the magnitude of effect sizes were previously unknown. In vivo studies were performed with different sample size based on animals availability and/or instructions from Ethical Authorities, in order to obtain the best statistical power possible. All n values are reported throughout the text.
Data exclusions	No data were excluded from the analyses unless technical mistakes or uncontrollable situations occurred that could result in inaccuracy, such as improper brain dissection/sectioning, food intake measurements with "spiller" mice, or low quality RNA extraction.
Replication	The major endpoints of the study (animal phenotypes, changes in neuron numbers) were replicated in independent cohorts of animals for most of the experiments. All attempts at replication were successful.
Randomization	In a context of transgenic VS wildtype animals, or in the within-subject design of the aMSH infusion study, randomization was not needed. The only experiment that required randomization was the fasting-refeeding experiment (4J-H), where animals were separated into random body-weight matched groups.
Blinding	The investigators were blinded to data collection and data analyses as animals were described using numbers throughout the procedures. The investigators only verified the identity of the animals at the data analysis step.

Reporting for specific materials, systems and methods

Materials & experimental systems

n/a	Involved in the study
<input type="checkbox"/>	<input checked="" type="checkbox"/> Unique biological materials
<input type="checkbox"/>	<input checked="" type="checkbox"/> Antibodies
<input type="checkbox"/>	<input checked="" type="checkbox"/> Eukaryotic cell lines
<input checked="" type="checkbox"/>	<input type="checkbox"/> Palaeontology
<input type="checkbox"/>	<input checked="" type="checkbox"/> Animals and other organisms
<input checked="" type="checkbox"/>	<input type="checkbox"/> Human research participants

Methods

n/a	Involved in the study
<input checked="" type="checkbox"/>	<input type="checkbox"/> ChIP-seq
<input checked="" type="checkbox"/>	<input type="checkbox"/> Flow cytometry
<input checked="" type="checkbox"/>	<input type="checkbox"/> MRI-based neuroimaging

Unique biological materials

Policy information about [availability of materials](#)

Obtaining unique materials	The only unique material in this manuscript is the newly developed Tbx3-Cre-Venus mouse. The authors will consider sharing this model with other teams if feasible.
----------------------------	---

Antibodies

Antibodies used

rabbit anti-Pomc precursor, Phoenix Pharmaceuticals H-029-30 polyclonal, lot 01800-1
 goat anti-Agrp R&D systems, AF634 polyclonal, lot CMH0717121
 chicken anti-GFP, Acris AP31791PU-N polyclonal, lot GFP879484,AR4_4-1-BT1(1)
 rabbit anti-Npy, Abcam ab30914 polyclonal, lot GR212905-1
 rabbit anti-Cart, Phoenix Pharmaceuticals H-003-62 polyclonal, lot 01251-8
 mouse anti-BrdU, Sigma B2531, lot BU-33 118K4835
 goat anti-Tbx3 Santa Cruz, sc-31656 polyclonal, lot E0613
 rabbit anti-Tbx3, Bethyl Laboratories A303-098A polyclonal 098A-1
 mouse anti-Bruchpilot, Developmental Studies Hybridoma Bank, DSHB Hybridoma Product nc82
 rabbit anti-Omb serum, Kind Gift from Dr. Gert O. Pflugfelder
 rabbit anti-cleaved caspase-3, Cell signaling 9664S 5A1E, lot 18082159

goat anti-Iba1, Abcam ab107519, lot GR3209946-1
 rabbit anti-GFAP, Dako, Z0334, lot 20040599
 chicken anti-vimentin, Abcam ab24525, lot GR3216660-8
 goat anti-GFP, Abcam, ab6673, lot GR287379-14
 rabbit anti-HA tag, C29F4, Cell signaling. lot 30021200

Validation

rabbit anti-Pomc precursor: validated by other users, cited 24 times in the company website.
 goat anti-Agrp: validated by other users, cited 13 times in the company website.
 chicken anti-GFP antibody: validated for IF by the company, and by users.
 rabbit anti-Npy: antibody validated for immunohistochemistry by the company, cited 18 times in the company website.
 rabbit anti-Cart: antibody validated for IF by the company, and by users, cited 18 times in the company website.
 mouse anti-BrdU: antibody validated for IF by the company, and by users (cited 157 times)
 goat anti-Tbx3: validated in the manuscript
 rabbit anti-Tbx3: validated in the manuscript
 rabbit anti-cleaved caspase-3: antibody validated for IF by the company, and by users (cited 1345 times).
 mouse anti-Bruchpilot: antibody validated by users (cited 385 times in www.citeab.com).
 rabbit anti-Omb serum: antibody validated by the generator.
 goat anti-Iba1, Abcam ab107519: antibody validated by the generator.
 rabbit anti-GFAP, Dako, Z0334: antibody validated by the generator.
 chicken anti-vimentin, Abcam ab24525: antibody validated by the generator.
 goat anti-GFP, Abcam, ab6673: antibody validated by the generator.
 rabbit anti-HA tag, C29F4, Cell signaling: antibody validated by the generator.

Eukaryotic cell lines

Policy information about [cell lines](#)

Cell line source(s)	ATCC
Authentication	performed by the source
Mycoplasma contamination	Cell lines were negative for mycoplasma
Commonly misidentified lines (See ICLAC register)	none

Animals and other organisms

Policy information about [studies involving animals](#); [ARRIVE guidelines](#) recommended for reporting animal research

Laboratory animals	We used C57BL/6 male mice. Age for each specific experiment is indicated in the manuscript. Age in pups varies from P0 to P4 and P14. Most of the experiments in adult mice were performed in 12-weeks old mice. Body weight and food intake curves in transgenic mice were obtained in animals ranging from 5 to 12 weeks of age. Body weight and food intake curves in AAV-treated mice were obtained in animals ranging from 12 to 19 weeks of age.
Wild animals	The study did not involve wild animals
Field-collected samples	The study did not involve samples collected from the field